Study of the Casimir-Lifshitz force in the plane-parallel geometry

Victoria Esteso Carrizo

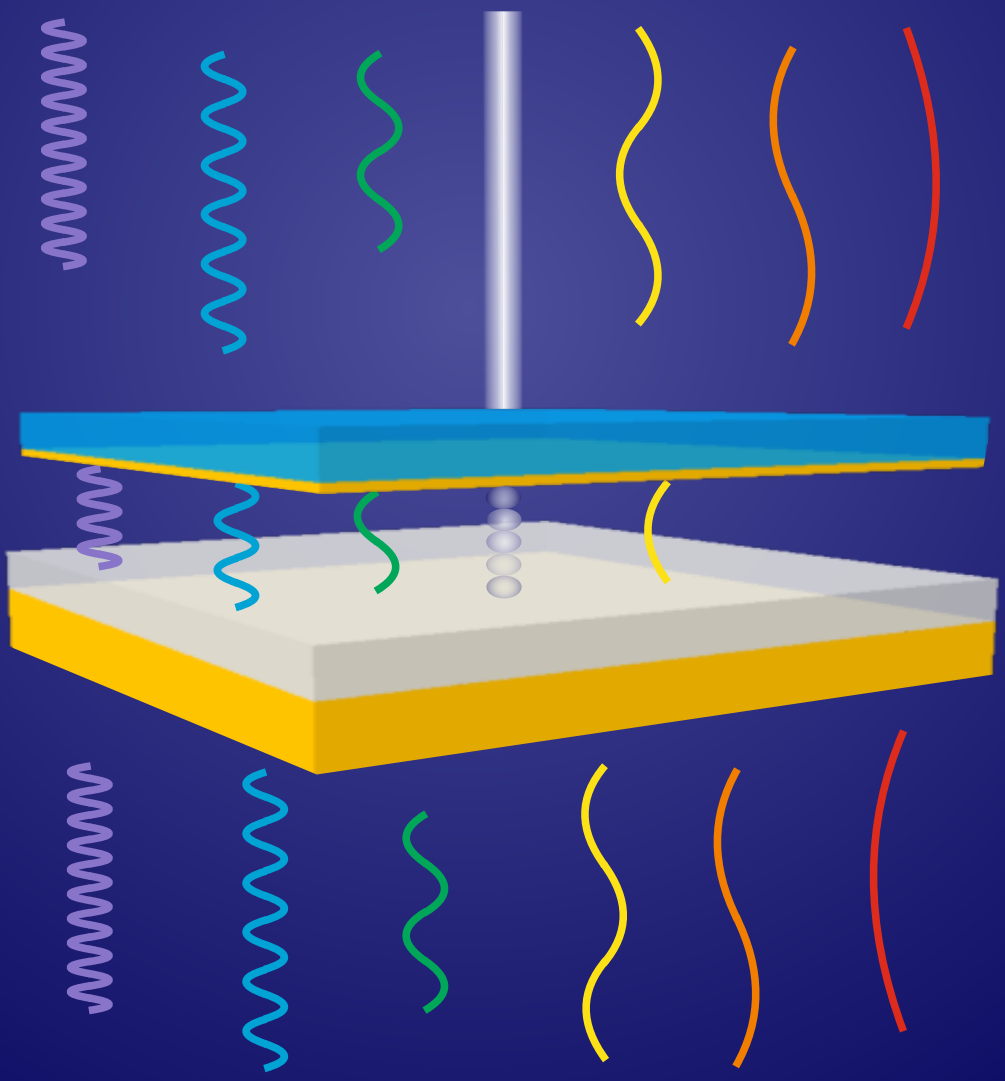

Study of the Casimir-Lifshitz Force in the plane-parallel geometry

A Dissertation
in Candidacy for the Degree of
Doctor of Philosophy

by

Victoria Esteso Carrizo

Dissertation Director: Prof. Hernán Ruy Míguez García
and Dr. Sol Carretero Palacios

Instituto de Ciencia de Materiales de Sevilla
Consejo Superior de Investigaciones Científicas

Departamento de Química Orgánica
Facultad de Química
Universidad de Sevilla

List of abbreviations

F_{C-L}	Casimir-Lifshitz force
F_g	Gravity force
F_B	Buoyancy force
F_{el}	Electrostatic force
EM field	Electromagnetic field
E field	Electric field
TE	Transversal Electric mode
TM	Transversal Magnetic mode
r	Simple Fresnel coefficient
R	Multiple Fresnel coefficient
j	Polarization index j = TM or TE
l	Layer material index
m	Matsubara frequency index
$\tilde{n}$	Complex refractive index
n	Real part of refractive index
k	Imaginary part of refractive index
ϵ_0	Static dielectric constant
ϵ	Dielectric function
$\hbar$	Reduced Planck constant
ω	Angular frequency
ξ	Matsubara frequency
T	Temperature

Δ	Increment in the contiguous magnitude
d_0	Separation distance between the thin film and the substrate or equivalently thickness of layer l = 0
MS	Multilayer Structure

Contents

1 Introduction **1**

1.1 Dispersion forces: from Casimir effect to Lifshitz theory 4

1.2 Casimir Effect 6

1.3 Casimir-Lifshitz force 8

1.4 Repulsive Casimir-Lifshitz force and levitation 11

1.5 Levitation phenomenon in the plane-parallel geometry . 14

1.6 Casimir-Lifshitz force and Materials Science 16

1.7 This thesis 18

2 Methods and Materials **20**

2.1 Expressions of the Casimir-Lifshitz force in the plane-parallel geometry 21

2.1.1 Rotation from real frequencies (ω) to Matsubara frequencies (ξ_m) at $T \neq 0$ K 23

2.1.2 Systems with arbitrary number of layers 28

2.1.3 Dielectric function of materials 30

2.1.4 Semi-analytical calculations 33

2.2 Electrostatic force 36

2.3 Roughness and patch potentials effect 37

2.4 Transfer Matrix Method 39

2.5 Field distribution and power absorbed 43

3 Levitation of thin films due to Casimir-Lifshitz interactions. Analysis of temperature effects **46**

3.1 Introduction 47

3.2 Levitation Phenomena in plane-parallel systems due to Casimir-Lifshitz and gravity force balance 47

3.3 Temperature dependence of equilibrium distance at room temperature 47

3.4 Simple rules to predict temperature variation effects on d_{eq} 47

3.5 Conclusions 47

4 Optical resonators based on Casimir-Lifshitz forces **48**

4.1 Introduction 49

4.2 Fabry-Pérot optical cavities 49

4.3 CasimirLifshitz Force Based Optical Resonators 49

4.4 High Q-factor optical resonators for accurate measurements of repulsive F_{C-L} 49

4.5 Effect of room temperature variations on the force balance and the optical cavity characterization 49

4.6 Conclusions 49

5 Optical Interference Effects on Casimir-Lifshitz Forces **50**

5.1 Introduction 51

5.2 Periodic multilayer structures and their optical response . 51

5.3 Effect of thickness and number of layers on Casimir-Lifshitz force 51

5.4 Tuning the Casimir-Lifshitz force with multilayer nanostructures 51

5.5 Conclusions 51

Bibliography **52**

Chapter 1

Introduction

It might sound surprising that the gecko's ability to adhere to surfaces [1], the friction that so often plagues tiny components in nanomachines [2, 3], the density anomaly of water [4], and the early stages of planets formation [5] have a common origin in the zero-point fluctuations of quantum fields [6]. These fluctuations are the basis of the weakest type of the interatomic and intermolecular forces which allow the formation of condensed matter, named dispersion forces [7]. Dispersion forces are inherently present in our daily life. In nature, they are at the heart of important phenomena in chemistry, physics and biology, being the cause of adhesion, surface tension, strength of solids and stability of both colloidal suspensions or biological membranes [8, 9, 10, 11], amongst others. They are also responsible for the organization of bio-systems like cellulose, lignin, and proteins, and they are the reason why geckos can climb in walls and ceilings [12, 13, 14, 15].

In nowadays technology, accelerometers integrated in smartphones or high precision positioning devices are examples of specialized cases in which dispersion forces play a main role, becoming more important as the distance between the interacting bodies is reduced [16, 17, 18, 19, 20]. Continuous miniaturization of devices has been a common fact in

the last decades. With this miniaturization, high accuracy in the control of forces acting on, for example, micro- and nanoelectromechanical systems (MEMS and NEMS), has become essential for their optimized design.

Another fascinating phenomenon fruit of the confinement of quantum fluctuations is the Casimir effect [21]. Briefly speaking, the Casimir effect occurs when two or more bodies are placed at nano- and micro-scale distances perturbing the available vacuum modes. Since the vacuum energy density varies when one of the objects is displaced with respect to the others, a force results. Such force is the so-called *Casimir force*. As it will be described in detail along this thesis, this force was originally predicted for perfectly conducting plates, but when realistic materials are considered, such force remains. In what follows, this force occurring amongst macroscopic bodies at nano- and micro-scale distances will generally be referred to as the *Casimir-Lifshitz* force, F_{C-L}.

In this regard, the influence of attractive F_{C-L} in NEMS and MEMS, which are the basis of computers, smartphones, and similar electronic devices, has been particularly analyzed in literature since they are the cause of main failures due to stiction between the components. One of the first evidences of this undesirable attractive interaction in devices was reported by Srivastava in 1985 [22], pointing that the Casimir-Lifshitz energy in the gate-region capacitor of a field-effect transistor device was 10 $\%$ of the electrostatic energy. By then, the scale of the systems was too large to have a critical impact, but nowadays, with the shrinking of devices, the role of the Casimir-Lifshitz interaction becomes decisive in the stability and device performance [16, 23, 24, 25]. Typically, the effect of F_{C-L} on micro and nanodevices is studied in simple systems like parallel plate capacitive switches (Fig. 1.1(a)), and cantilevers (Fig. 1.1(b)). In them, external forces such as F_{C-L} or electrostatic forces, affect the dynamic of a movable part of the device which in turn is restored to its original position due to an elastic force. The stability is given by the balance between the elastic force and the applied external forces, and when the

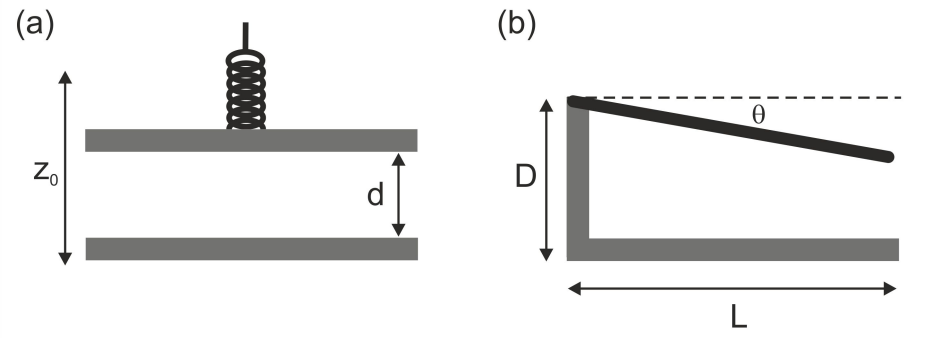

Figure 1.1: (a) Scheme of a MEMS consisting on a plane-parallel capacitive switch with one of the plates attached to a spring. (b) Scheme of a cantilever deflected an angle θ with respect to a reference position when no external forces are applied.

latter overcomes the former, the movable part collapses and irreversible adheres to the opposite surface. This phenomenon is known as *jump into contact* and results in the uselessness of the device. Repulsive Casimir-Lifshitz interactions or reducing the attractive intensity of F_{C-L} could avoid adhesion and permanent stiction between movable parts in devices. Because of that, a deep knowledge of the underlying fundamental concepts of such forces is essential for understanding nature mechanisms, as well as for the future of advanced technologies, such as MEMS and NEMS, optoelectromechanics and microfluidic devices, sensors, or optical communications.

Recent experimental advances have allowed acquiring novel insight into the nature of such dispersion forces [26] while proving their potential to attain quantum levitation between macroscopic bodies [27], settling this topic in the focus of the scientific community and making the comprehension of this quantum interaction essential for the development of the forthcoming tinier technology.

Interestingly, the nature (attractive or repulsive) and strength of the

Casimir-Lifshitz force can be engineered, amongst others, through the optical properties of the interacting materials, a characteristic that makes it specially attractive from the Materials Science point of view. The aim of this thesis is to exploit theoretically the possibilities of the Casimir-Lifshitz interaction in the plane-parallel geometry when a fluid material mediates the interaction by tuning and designing the optical characteristics of the interacting plates.

In what follows, a deep analysis of the relevance of the optical properties of the materials involved on the Casimir-Lifshitz interaction in the plane-parallel geometry is presented.

1.1 Dispersion forces: from Casimir effect to Lifshitz theory

Apart from the ionic and covalent bonds, between two neutral atoms or molecules (without net electrical charge), there is also a much weaker binding force commonly named *van der Waals force*. Typically, these kinds of forces are classified in three types: (a) Kessom forces, between atoms or molecules with permanent electric dipoles, (b) Debye forces, between an atom or molecule with permanent dipole and a neutral atom or molecule, and (c) London forces, between two neutral atoms or molecules without permanent dipole moment that instantaneously acquire a dipolar moment (a quantum mechanical phenomenon) and interact with each other. This last type of forces are also named *dispersion forces*, since their average dipolar moment is zero but the dispersion of the values is non-zero.

Dispersion forces may become very intense at the nano- and micro-scale, depending on the number of atoms or molecules involved and their polarizabilities, as well as the geometry of the system and the temperature. The origin of these forces lays on the fact that vacuum, despite the absence

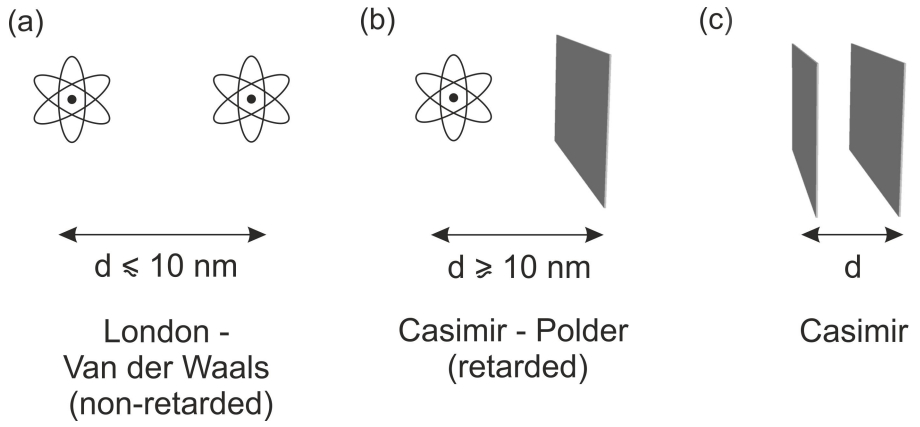

Figure 1.2: Schematics of the different types of dispersion forces: (a) non-retarded London-van der Waals, (b) retarded Casimir-Polder and (c) Casimir interaction.

of matter and radiation, is not empty. According to quantum field theory, vacuum may be described as a quantized electromagnetic (EM) field, that is, as a set of oscillators of all frequencies (ω). This implies that the energy at the ground state of one of those harmonic oscillators is not zero, and instead, it takes the value $\hbar\omega/2$ meaning that vacuum has an energy density different from zero which is the basis of the quantum fluctuations [6, 28].

The attraction between two atoms or molecules is attributed to the instantaneous dipolar moment produced by the moving electrons clouds (due to quantum fluctuations). This instantaneous dipolar moment produces fluctuating EM fields that, in turn, induce an instantaneous dipolar moment in the other atom or molecule, and vice-versa. In average, the dipolar moment of the atom or molecule is zero, but in the quantum theory developed by London in 1930 [29], the dispersion of the dipolar moment operator is distinct from zero, leading to correlations between the EM field fluctuations generated in both atoms or molecules.

When the atoms or molecules are close enough, the correlation be-

tween the oscillations of the instantaneous dipole and the induced dipole does not depend on the speed of light (c) anymore, being a simultaneous interaction named *non-retarded London - van der Waals force*, (sometimes literature also refers to this non-retarded interaction just as van der Waals force). As the separation between atoms or molecules becomes larger, typically larger than 10 nm, the correlation of the oscillating electronic clouds depends on the time the interaction takes to propagate, inversely proportional to c, leading to relativistic retardation effects first studied by Casimir and Polder between an atom and a wall [30]. That interaction is known as the *Casimir-Polder force*. After this result, Casimir applied the same idea to describe theoretically the attraction between two perfectly metallic plates in vacuum [21], what is known as *Casimir Effect*. Figure 1.2 shows schematics of canonical systems displaying the three types of dispersion forces: (a) the London - van der Waals force, (b) the Casimir-Polder force, and (c) the Casimir force

1.2 Casimir Effect

In 1948, Casimir theoretically predicted that two perfectly conducting metallic plates, in vacuum, at 0 K, and separated at nano- and microscale distances are strongly attracted as a consequence of the quantum fluctuations of the EM field in vacuum [21]. As it was previously pointed out above, the origin of the *Casimir Effect* is the quantum fluctuations of the EM field, which can be seen as temporal changes of the vacuum energy at a point in space, or as virtual photons that appear and disappear in vacuum instantaneously, without contradicting Heisenberg's uncertainty principle, $\Delta E \Delta t \geq \hbar/2$. The cavity formed by the perfectly conducting plates considered by Casimir are boundaries in the space that limit the EM field fluctuations between them, i.e., those boundaries limit the possible energy or wavelength values that can exist inside the cavity, discarding longer enough wavelengths that do not fit inside the cavity (see scheme

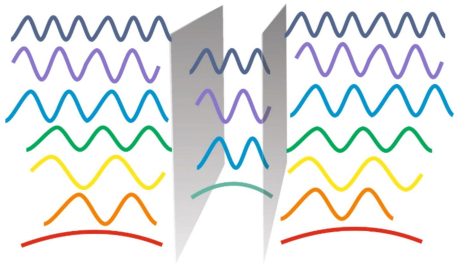

Figure 1.3: Scheme of the Casimir effect between two perfectly metallic plates in vacuum.The unbalanced EM field inside and outside the cavity causes an effective attraction of the plates.

in Fig. 1.1). The unbalanced EM field inside and outside the cavity gives rise to a difference of radiation pressure on each face of the plates, causing an effective attraction of the same. Such attractive force is the so-called *Casimir force* and its effect is a macroscopic manifestation of the quantum field theory. Casimir developed this idea when dealing with the stability of colloidal suspensions in water, in which each particle repels and attracts each other due to electrostatic and van der Waals forces, respectively. He was trying to address the different power laws for the attractive force between particles at short and long separation distances, when he came up with the idea that the presence of two large particles (boundaries) would modify the quantum fluctuations of EM field in the space between them. Linking this idea with the simplest system of two perfectly metallic plates in vacuum, he obtained the mathematical expression for the force per unit area (F_C) between the infinitely thin plates separated a distance d in the micro and nanoscale:

$$F_C = -\frac{\pi^2 \cdot \hbar c}{240 \cdot d^4} \tag{1.1}$$

The above expression, which gives the force in units of N/m^2, simply depends on the separation distance between the plates and universal

constants, $\hbar$ and c proving the quantum and relativistic nature of the force, whose intensity rapidly decays with d and is negative for attractive forces. To show the order of magnitude of the force per unit area, for separation distances of d = 10 nm, a force per unit area of $F_C \approx 1.3$ atm is attained. For simplicity, and following the terminology commonly employed in the Casimir-Lifshitz scientific community, in this thesis the word 'force' will refer to a 'force per unit area'.

Although nowadays the Casimir effect is well accepted and used in diverse fields like condensed matter physics, quantum field theory, mathematical physics and renormalization techniques, quantum chromodynamics or cosmology, it took nearly six decades since the theoretical prediction of Casimir to have sufficiently precise and conclusive experimental measurements to demonstrate its existence. Later on, Lifshitz, initially using fluctuating fields [31], and afterwards in collaboration with Dzyaloshinskii and Pitaevskii employing the quantum field theory [32], developed in a couple of seminal papers a unified theory describing simultaneously the non-retarded London-van der Waals interaction in the limit of rarefied medium and short separation distances, $d \leq 10$ nm (see schematics in Fig. 1.2 (a)), the retarded Casimir-Polder interaction between an atom and a wall for larger separation distances, $d \geq 10$ nm (Fig. 1.2 (b)), and the Casimir effect for two metallic plates with $\varepsilon \to \infty$ (Fig. 1.2 (c)). Moreover, this generalized theory describes the force amongst objects of arbitrary shape made of realistic materials and at any temperature.

1.3 Casimir-Lifshitz force

The Casimir force expressed in Eq. 1.1 describes the interaction between two perfectly metallic plates. When realistic materials (presenting losses at specific frequencies) are considered, the force persists, but such description is not accurate anymore. In order to take into account

losses of metals and dielectric macroscopic materials, Lifshitz extended the Casimir theory and included in his formalism [31] the complex dielectric function, ε = $\varepsilon'(\omega)$ - i $\varepsilon''(\omega)$, accounting for dispersion and absorption optical properties. Since then, the interaction was known as Casimir-Lifshitz force (F_{C-L}). In his theory, Lifshitz described the long-range interaction between diverse materials as a consequence of the correlation of fluctuating EM fields which exist inside the materials and extend beyond their boundaries. To develop the theory, Lifshitz solved Maxwell's equations for macroscopic materials at T = 0 K, and introduced the fluctuation-dissipation theorem [6], which states that the correlations of the fluctuating EM fields, expressed in terms of the electric field $\overrightarrow{E}$, are directly proportional to the dissipation of the materials ε'':

$$\langle E_i(r)E_j(r')\rangle = 2\hbar\varepsilon''(\omega)\delta_{i,j}\delta^3(r-r') \tag{1.2}$$

In the above expression, $\langle ...\rangle$ denotes spatial average, i and j run over the x, y and z field components, r and r' denote points in space, and δ stands for the Dirac delta function. Interestingly, the strength of the force depends on the reflectivity of the interacting surfaces, being stronger for higher reflectance surfaces. Most metals are excellent broadband reflectors, and thus, the interaction between metallic plates is usually much stronger than that between dielectrics. However, as it will be shown in detail in Chapter 2, because the force is extremely broadband, the fact that a material is transparent in the visible spectrum does not necessarily mean that it will present a reduction of the force intensity. Moreover, the contributions of frequencies to F_{C-L} are highly oscillatory, and include both attractive and repulsive components [33, 34], hindering the calculations concerning numerical convergence, and blocking intuition from optics in order to tune the intensity and nature of the interaction with materials optical properties.

Lifshitz theory is also valid for bodies of arbitrary shape, despite an

analytical expression is only provided for the plane-parallel configuration. For curved surfaces, for instance, as that would be the case of colloidal particles or gas bubbles, it is possible to use the so called *proximity force approximation* (PFA) which was first applied by Derjaguin and collaborators [35] in F_{C-L} measurements between two fused quartz surfaces, one flat and the other with spherical shape. They showed that the force acting between a plate and a body of finite curvature can be expressed in terms of the force between two planar semi-infinite walls. It was also demonstrated that the force is much more intense in the plane-parallel configuration than in geometries incorporating spheres.

The first experimental attempt to measure the Casimir-Lifshitz force with real materials was reported by M. Sparnaay in 1958 [36], who observed, through capacitance measurements, the attractive force between pairs of metallic plates made of aluminium, chromium, and steel and chromium. However, results were not conclusive due to, among other difficulties, the inaccuracy in the plates alignment. Such difficulty was overcome by Dejarguin and co-workers [35], by considering curved surfaces of different radii to avoid limitations on the parallelism between the interacting bodies. After some other attempts without conclusive measurements of the Casimir-Lifshitz force[37, 38, 39], some relevant experimental results were finally attained several decades after the theoretical prediction thanks to the improvement in precision and sensitivity of the techniques employed. Some examples are the experiments by S. Lamoreaux et al. [40], who measured the force between a lens and a plate both coated with gold, using a torsion pendulum; by U. Mohideen et al. [41], who employed for the first time an atomic force microscope and measured the force between a sapphire plate and a sphere attached to the cantilever coated with metals such as aluminium, chromium and gold; or the work by by R. Decca et al. [42], who achieved the highest experimental precision of the Casimir-Lifshitz force employing a micromechanical torsional oscillator. Interestingly, the spanning of the Casimir-

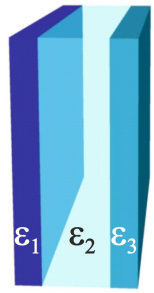

Figure 1.4: Scheme of a plane-parallel system with a material (that might be different from vacuum) between the interacting bodies.

Lifshitz interaction to current technologies was reported in 2001 with the first MEMS actuated by F_{C-L} [43]. In fact, few examples demonstrating repulsive Casimir-Lifshitz forces have been reported, being one of the reasons the lack of knowledge about the value of the dielectric permittivity at 'all' frequencies (essential for evaluation of Casimir-Lifshitz forces), which is only known for a few solids and liquids. Among them, a limited number of material combinations that are chemically stable when arranged together may display repulsive forces of this kind. Additional outstanding experimental demonstrations of thermal contributions to the Casimir-Lifshitz force [44] and the critical Casimir force [45] were also achieved in the following decade. Further details about the experimental force measurements progress including real materials are provided in Chapter 4.

1.4 Repulsive Casimir-Lifshitz force and levitation

One of the most interesting results derived from the Lifshitz theory is the fact that F_{C-L} may be repulsive, having important implications in

fundamental physics and technology [32, 46, 47], since, for instance, it would prevent adhesion and stiction between movable parts in NEMS and MEMS which are the reason of main failures in this kind of devices [48, 3]. Moreover, the possibility of having repulsive F_{C-L} rapidly led to the idea of *quantum trapping*, a phenomenon in which F_{C-L} evolves from repulsion to attraction as the separation distance between bodies increases. Moreover, if the repulsive F_{C-L} is strong enough to counteract the effect of gravity if the system is in presence of the gravitational field, *quantum levitation*, might occur.

Until the extended theory was developed, the Casimir-Lifshitz interaction was predicted to be always attractive between parallel plates, typically separated by vacuum or air (i.e $\varepsilon'' = 1$). Actually, the interaction between two plates made of the same material will always be attractive. Several approaches might be applied to obtain repulsive Casimir-Lifshitz forces between two bodies in vacuum. Examples cover the consideration of interacting objects with alternative geometries, such as an elongated metallic particle approaching a metal plate with a hole drilled on it [49], the employment of metamaterials, like chiral or magnetodielectric metamaterials carefully designed [50], or the operation with materials whose dielectric functions fulfill certain relations, as it will be extensively explained in the coming sections. This thesis will focus on the latter approach and will consider the plane-parallel geometry based on stratified realistic materials having a liquid medium between the interacting plates. Figure 1.4 displays a scheme of a general plane-parallel system consisting of two bodies whose dielectric functions are ε_1 and ε_3, separated by a liquid with ε_2. According to Lifshitz results, repulsive forces might be attained if the dielectric function of the interacting materials fulfill one of the following conditions:

$$\varepsilon_1 < \varepsilon_2 < \varepsilon_3 \tag{1.3}$$

or

$$\varepsilon_1 > \varepsilon_2 > \varepsilon_3 \tag{1.4}$$

Importantly, these conditions must be satisfied in a wide range of the so-called Matsubara frequencies (further details are provided in Chapter 2). In short, an integral over the full spectral frequency range ($\omega \in [0, \infty]$) of the dielectric function of materials is computed, making it difficult to find combinations of materials that obey the previous conditions.

The first experimental results of repulsive Casimir-Lifshitz interactions were measured six decades after the theoretical prediction with the use of an atomic force microscope (AFM) between the tip of the cantilever, or a sphere attached to it, and a flat substrate, all immersed in a liquid at small separation distances (below 10 nm) [51, 52, 53, 54, 55]. It was also demonstrated that the inclusion of a fluid different than air between the interacting materials decreased the intensity of the force [56].

For larger separations distances, above tens of nanometers, repulsive F_{C-L} was first theoretically predicted [57] and afterwards measured with the use of an AFM [58] between a gold sphere and a silica substrate all drowned in bromobenzene. Several considerations were needed to successfully perform this experiment: i) calibrating the AFM measurements in liquids [56], ii) studying the effect of discrepancies among theoretical and real dielectric properties of materials [59], and iii) analyzing the effect of residual electrostatic forces [60].

Most of the experimental measurements of repulsive F_{C-L} were performed in the sphere-plane geometry in order to avoid alignment problems. Concerning the plane-parallel geometry, the first experimental evidence was recently attained [27] by using a completely different approach based on spectroscopic measurements in a quantum trapping scenario. In it, an optical resonator was built with a thin metallic film immersed in a fluid over a substrate due to the balance of gravity and repulsive F_{C-L}. Casimir-Lifshitz forces were indirectly attained through reflectance measurements by adjusting the equilibrium distance at which the metallic film

levitated.

All those advances prove the possibility of manipulating the strength and nature of F_{C-L}, shedding light on fundamental aspects of F_{C-L} and laying the groundwork for technological applications. Particularly, stable quantum levitation can be used as a platform for a variety of applications such as contact-free nanomachines, ultrasensitive force sensors, and nanoscale manipulations. Next, levitation will be deeply analyzed in a plane-parallel geometry.

1.5 Levitation phenomenon in the plane-parallel geometry

Let us consider a simple plane-parallel system with two plates (one of them a self-standing thin film) facing each other in a fluid as it is displayed schematically in Fig. 1.5. Typically, the thickness of the thin film (d) and the separation distance (d_0) between it and the substrate, range from tens to hundreds of nanometers. In this simple case, it is considered that the forces acting on the thin film are gravity (F_g), buoyancy (F_B), and F_{C-L}. It might also be taken into account the effect of other forces acting on the system, such as the double layer force (F_{dl}), arising near charged surfaces in liquid solution, or the effect of surface roughness and patch potentials, described in detail in Section 2.2 and Section 2.3, respectively. However, for the sake of simplicity, in what follows, those effects will be neglected to analyze fundamental concepts of the levitation phenomenon. Definitions of F_g, F_B, and F_{C-L} are given in Eq. 1.5, 1.6, and Eq. 2.1 (extensively explained in Section 2.1), respectively.

$$F_g = -g\rho_{film}d \tag{1.5}$$

$$F_B = g\rho_{fluid}d \tag{1.6}$$

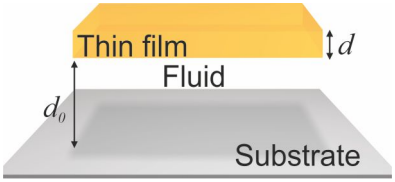

Figure 1.5: Scheme of a plane-parallel system consisting of a self-standing thin film of thickness d immersed in a fluid standing above a substrate at a separation distance d_0.

In the above expressions, g is the standard gravity, and ρ_{film} and ρ_{fluid}, the density of the suspended film and the fluid, correspondingly. Note that units of ρ are kg/m because of the infinite area considered of both the substrate and the thin film. Following the sign convention of the Casimir effect, positive values of the force correspond to repulsive forces, and negative ones to attractive F_{C-L}. The expression of the force balance at equilibrium is then given by:

$$F_T(d_{eq}, T) = F_g + F_B + F_{C-L}(d_{eq}, T) = 0 \tag{1.7}$$

with F_T the total force acting on the suspended film, and d_{eq} the equilibrium separation distance at which the thin film stands over the substrate in thermal equilibrium at a fixed temperature, T.

In Eq. 1.7, the balance of forces is zero and the system is at mechanical equilibrium. This equilibrium can be either stable or unstable, depending on the sign of the forces acting on the thin film. Figure 1.6 illustrates both scenarios of stability. Panel (a) displays a situation in which the suspended film is at stable equilibrium. In this case, the density of the levitating film is higher than that of the fluid, and so, the intensity of gravity is larger than that of the buoyancy force. In this situation, if the thin film approaches the substrate, the repulsive F_{C-L} restores the equilibrium position d_{eq}, whereas, if the thin film moves away from the substrate, F_g brings it back to d_{eq}. Panel (b) presents the opposite case, in which F_{C-L}

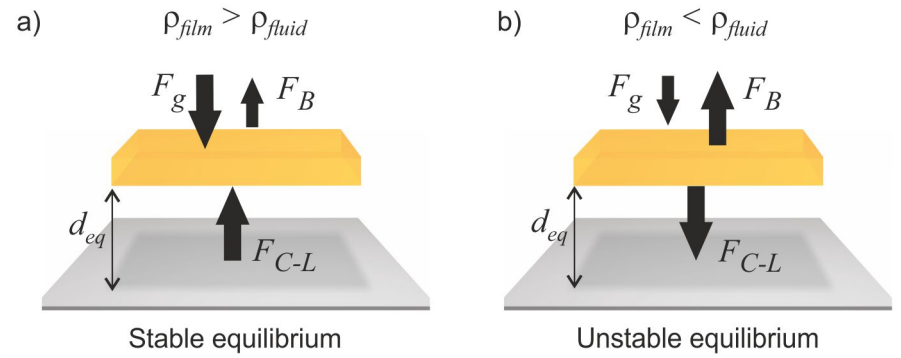

Figure 1.6: (a) Stable equilibrium distance (b) Unstable equilibrium distance.

between the thin film and the substrate is attractive, but the buoyancy force compensates both gravity and F_{C-L}, as the density of the fluid is larger than that of the thin film. In this case, the system is at an unstable equilibrium position, and if the film deviates from d_{eq} it will stick to the substrate due to the attractive F_{C-L} if $d_0 < d_{eq}$, or it will float if $d_0 > d_{eq}$.

In this thesis, the balance of F_{C-L}, F_g, and F_B is theoretically analyzed in plane-parallel geometries based on stratified materials that can be easily found in nature and whose dielectric functions relations enable repulsive Casimir-Lifshitz forces.

1.6 Casimir-Lifshitz force and Materials Science

Materials Science is an interdisciplinary branch of Science based on Physics, Chemistry and Engineering, focused on the development of novel materials. Originally, Material Science was devoted to the study of metallurgy an ceramics, focusing on the relation between the process of fabrication, the microstructure and the resulting properties of materials. However,

soon those analyses were extended to all kinds of materials, including semiconductors, polymers, biomaterials, nanomaterials, and optical and magnetic materials, among others. Designs of such materials are commonly inspired by the surrounding world, mimicking or reproducing the same structures or complexity found in nature, but also new materials are created by adding advanced functionalities to the already existing ones.

Examples of outstanding materials developed in Material Science are graphene [61], furellenes [62], photonic and acoustic crystals [63, 64], doped semiconductors with desired electronic properties[65], perovskites [66], biocompatible polymers [67], quantum dots [68], spin valves [69], and a large etcetera, which have applications on diverse fields such as photovoltaics [70], tissue regeneration [71], magnetic storage [72], drugs delivery [73], light emitting devices [74] or quantum computation [75].

Of particular interest for the thesis work herein presented are the multifunctional optical materials. Materials with designed and engineered optical properties have allowed the control of the absorption, emission or propagation of light in optical fibers [76], wave guides [77], antireflecting coatings [78], plasmonic structures [79], photonic crystals [80] or negative refractive index materials [81].

The possibility of tailoring electromagnetic boundary conditions enables a variety of optical phenomena and related applications, and in addition, it allows to engineer dispersion forces, such as the Casimir-Lifshitz force. Particularly, the intensity and nature of F_{C-L} can be tuned by controllably modifying the optical properties of the interacting materials. In this regard, optical design may allow the development of materials with specific functionalities and characteristics, allowing a further comprehension of the underlying physical and chemical processes in dispersion forces. For instance, based on attractive van der Waals forces, Material Science has allowed the creation of bio-inspired materials that let humans climb vertical walls as geckos do [82], and new functionalities have been added to already existing nanomachines designed to be

driven by the Casimir-Lifshitz force [43].

However, as it was mentioned before, it is not straightforward to find combinations of materials presenting repulsive F_{C-L} as intuition cannot be applied when Matsubara frequencies are computed. Moreover, since the dielectric function of all materials in the system need to be known over an 'infinite' frequency range, restrictions on the possible materials to be employed are maximized. Ultimately, these compact materials must be chemically compatible with the fluid in which they are immersed, and their thickness need to be easily determined in plausible experiment. Different examples of materials combinations have been proposed in literature [83, 84, 85], including the use of chiral materials[86, 87, 88], magnetodielectric metamaterials [50, 85, 89], superconductors [90], and graphene [91].

In the same direction, another important challenge is to reduce the strength of the attractive interaction to maximize the durability of MEMS and NEMS. Many different approaches have been proposed in literature, such as nanostructuring the surface of materials [92], modifying the dielectric function of materials by changing the crystalline phase with temperature [93], through the change of the carrier density shining silicon [94, 95] or by means of external magnetic fields [96].

1.7 This thesis

This thesis tackles the theoretical study of the Casimir-Lifshitz force in the plane-parallel geometry from the Materials Science point of view, paying specific attention to the optical properties of the interacting materials. The main interest will be to control the intensity and sign of F_{C-L}, but also to find novel material designs that will provide insight into the underlying fundamental physics, with potential applications in nanotechnology.

This thesis has a profound theoretical basis, but the systems under

study have been conceived bearing in mind potential experimental applications, i.e., taking in consideration available materials and optical characterization techniques. The devised self-standing thin films (in both single or multilayer configurations) need to be compact, mechanically stable, of smooth surfaces, of controlled thickness, and chemically compatible with the fluid in which they are immersed.

In Chapter 2, the theoretical tools used along the thesis are presented. Specifically, the methods applied for the calculation of F_{C-L} in the plane-parallel geometry and for the simulation of the optical response of the systems studied are described. The Lifshitz expression for the F_{C-L} and the Transfer Matrix method will be discussed in detail. Furthermore, semi-analytical calculations of the EM field and the spatial distribution of absorption inside the optical materials under consideration are explained.

In Chapter 3, the effect on F_{C-L} of temperature variation around room temperature has been investigated in systems which present levitation due to repulsive F_{C-L}. At the end of the chapter, the connection between the effect of temperature variations and the intrinsic optical properties of the materials forming the system is analyzed.

In Chapter 4, based on the levitating systems analyzed in Chapter 3, a careful design of an optical resonator is carried out in order to propose a levitating system in which measurements of repulsive F_{C-L} are possible through optical spectroscopy. In addition, the effect of temperature in this levitating system is analyzed.

In Chapter 5, the focus is put on how to control the strength and nature (attractive or repulsive) of the F_{C-L} by nanostructuring onoe of the interacting planar bodies. The geometrical parameters of the nanostructure allows to tune F_{C-L} in intensity and sign, and its variations are explained in terms of the optical interference occurring inside the material, which gives rise to specific EM field distribution and absorption profiles inside the nanostructure.

Chapter 2

Methods and Materials

This chapter is devoted to the description of the expressions used in the calculations of the forces acting on the systems here considered, and the optical response of the same structured systems. First of all, the expression of the Casimir-Lifshitz force (F_{C-L}) for the plane-parallel geometry is presented, detailing important aspects such as the form it takes for T = 0 K and T $\neq$ 0 K; the rotation from real frequencies (ω) to Matsubara frequencies (ξ); and the importance of the dielectric function of materials involved in the resulting F_{C-L}. In addition, an example reproducing results from literature will be also presented. Then, the theory of the double-layer force (F_{dl}) is presented and the effect of surface roughness and patch potentials is reviewed. Finally, regarding the optical response of generalized multilayer structures, the Transfer Matrix Method is detailed, which in turn allows to extract information about the distribution of the EM field and the power absorbed in each layer of the system.

2.1 Expressions of the Casimir-Lifshitz force in the plane-parallel geometry

The expression of the Casimir-Lifshitz force can be derived following two formalism. The first one consists in solving the Maxwell's equations for macroscopic materials, calculating the Maxwell stress tensor ($\mathcal{T}$) by using the fluctuation-dissipation theorem, and finally taking the average of the zz-component $\langle \mathcal{T}_{zz} \rangle$ written in terms of Green functions. Another approach considers the fully quantum nature of EM fields. In it, the difference in energy inside and outside the cavity formed by two bodies interacting is calculated by solving the eigenvalues of the modes allowed inside it. Originally, Lifshitz attained the closet expression for the plane-parallel geometry, known as *Lifshitz formula*, from $\langle \mathcal{T}_{zz} \rangle$ for a system like the one depicted in Fig. 2.1. In it, ε_l is the dielectric function of the corresponding l material, with l = 1 and l = -1 that of the interacting plates, and l = 0, the material mediating the interaction [31]. The distance between the semi-infinite bodies or, equivalently, the thickness of the material mediating the interaction is denoted by d_0 and $r_j^{(0,1)}$ and $r_j^{(0,-1)}$ stand for the simple Fresnel reflection coefficients of the top and the bottom interface of material l = 0, for polarizations $j = TE, TM$. One of the most common versions of the Lifshitz force expression at $T = 0$ K in a system like the one just described is given by the following equation [28]:

$$F_{C-L}\left(d_0\right) = -\frac{\hbar}{2\pi^2}\int_0^\infty k_\perp \, dk_\perp \int_0^\infty d\omega \; Im\left\{ k_0 \sum_{j=TE,TM} \left[\frac{e^{2k_0 d_0}}{r_j^{(0,1)}(\omega, k_\perp)\cdot r_j^{(0,-1)}(\omega, k_\perp)} - 1 \right]^{-1} \right\} \quad (2.1)$$

In the above expression, $\hbar$ is the Planck constant and k_0 is the wavevec-

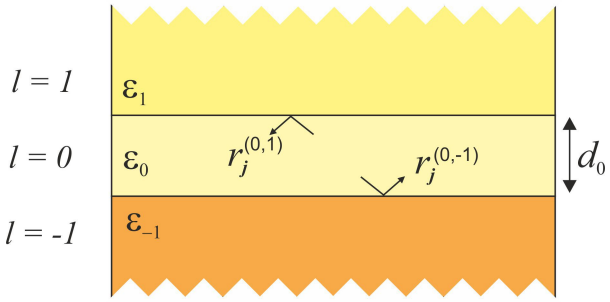

Figure 2.1: Scheme of two semi-infinite materials (l = 1 and l = -1) interacting by Casimir-Lifshitz force through material l = 0, which mediates the interaction. Each material l is described by its dielectric function ε_l whereas the thickness of material l = 0, or equivalently, the separation distance between the semi-infinite bodies, is given by d_0. $r_j^{(l,l')}$ denotes the simple Fresnel coefficient at the interface between materials l and l'.

tor component inside the mediating material, perpendicular to the interfaces. Also, k_0 is is the wavenumber in the plane of the planar surface at the interface, also perpendicular to $\mathbf{k}_\perp = (k_x, k_y)$. The expression for k_l is written as

$$k_l = k_l(\omega, k_\perp) = \left[k_\perp^2 - \varepsilon_l(\omega)\frac{\omega^2}{c^2}\right]^{1/2} \tag{2.2}$$

with c the speed of light. In addition, the simple Fresnel reflection coefficients in Eq. 2.1, $r_{TM}^{(0,\pm1)}$ and $r_{TE}^{(0,\pm1)}$ are defined as:

$$r_{TM}^{(0,\pm1)}(\omega, k_\perp) = \frac{\varepsilon_{\pm1}(\omega)k_0 - \varepsilon_0(\omega)k_{\pm1}}{\varepsilon_{\pm1}(\omega)k_0 + \varepsilon_0(\omega)k_{\pm1}} \tag{2.3}$$

$$r_{TE}^{(0,\pm1)}(\omega, k_\perp) = \frac{k_0 - k_{\pm1}}{k_0 + k_{\pm1}} \tag{2.4}$$

Numerically, the evaluation of Eq. 2.1 is not trivial, as it depends exponentially on $k_0(\omega, k_\perp)$. According to Eq. 2.2, in the simplest case in which $\varepsilon_0 = 1$, k_0 can take pure real values (if $|k_\perp| \geq \omega/c$) or pure imaginary values (if $|k_\perp| < \omega/c$) leading, in the last case, to a complex exponential function with rapid oscillations difficult to deal with computationally.

Lifshitz extended his formalism to include thermal fluctuations always present at $T > 0$ K [31], something necessary to describe, for example, experiments at room temperature. The following subsection addresses this extension and describes the modifications to the original expression given by Eq. 2.1.

2.1.1 Rotation from real frequencies (ω) to Matsubara frequencies (ξ_m) at $T \neq 0$ K

Let us consider first the case of a system at $T = 0$ K.

Rapid oscillations take place in the integrand of Eq. 2.1 for T = 0 K, complicating the computation of F_{C-L}. To avoid them, a closed integral in the complex plane can be performed. By doing so, the available frequencies are now expressed as a complex variable $\Omega = \omega + i\xi$, where ω and ξ are the corresponding real and imaginary parts.

According to Cauchy's theorem, the closed integral ($\oint$) of any function $f(\Omega)$ analytic in a region of the complex plane, for instance in the first quadrant of the Ω complex plane, fulfills that

$$\oint_C d\Omega f(\Omega) = 0 \tag{2.5}$$

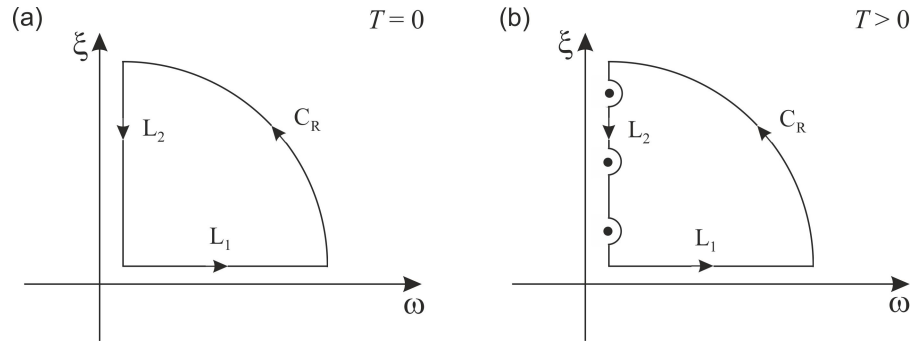

Figure 2.2: Scheme of the closed path in the complex plane $\Omega = \omega + i\xi$, for (a) T = 0 K and for (b) $T > 0$ K. Each closed path consist of three segments: L_1, L_2 (straight) and C_R (circular). In panel (b) at $T > 0$ K, the integrand presents poles on the ξ-axis causing a slightly change in the closed path.

where C is an arbitrary closed path lying within that region of the complex plane in which $f(\Omega)$ is analytic. In the example presented in Fig. 2.2(a), the closed path C consists of three segments, two straight and one circular, denoted as L_1, C_R and L_2. Specifically, L_1 corresponds to a segment along the positive real axis (0,∞), C_R is the 90º arc with infinite radius from the positive real axis to the positive imaginary axis, and L_2 runs along the positive imaginary axis ($i\infty$,0). However, in panel (b), at $T > 0$ K, the closed path slightly changes as a consequence of the poles that are introduced by the integrand in the ξ-axis, as it will be explained below. [28, 97].

If $f(\Omega)$ vanishes in the arc, and it is real for $f(i\xi)$, as it has been demonstrated for the integrand in Eq. 2.1 [28, 97], then

$$Im \int_0^\infty d\omega f(\omega) = \int_0^\infty d\xi f(i\xi) \tag{2.6}$$

Therefore, Eq. 2.1 can be rewritten as

$$F_{C-L}\left(d_0\right) = -\frac{\hbar}{2\pi^2}\int_0^\infty k_\perp\, dk_\perp \int_0^\infty d\xi$$
$$k_0 \sum_{j=TE,TM}\left[\frac{e^{2k_0 d_0}}{r_j^{(0,1)}(i\xi,k_\perp)\cdot r_j^{(0,-1)}(i\xi,k_\perp)} - 1\right]^{-1} \tag{2.7}$$

with k_l expressed in terms of $i\xi$ and $k_\perp$

$$k_l = k_l(i\xi,k_\perp) = \left[k_\perp^2 + \varepsilon_l(i\xi)\frac{\xi^2}{c^2}\right]^{1/2} \tag{2.8}$$

and with

$$\varepsilon_l(i\xi) = 1 + \frac{2}{\pi}\int_0^\infty \frac{\omega\varepsilon_l''(\omega)}{\omega^2+\xi^2}\, d\omega \tag{2.9}$$

Note that $\epsilon_l(i\xi)$ is real for every $i\xi$ value. Observe also that k_l(iξ,$k_\perp$) is real for any $i\xi$ and $k_\perp$ values involved in Eq. 2.7, eliminating the complex exponential from the integrand and, consequently, the rapid oscillations in Eq. 2.7. At this point, I would like to bring your attention to the limits of integration in Eq. 2.9. They are defined from 0 to ∞, which is a real challenge from the experimental point of view, as dielectric functions must be known for such a frequency range. However, using data in a sufficiently wide spectral range, which must include main absorption bands, usually results in a good approximation of the integrated dielectric function.

In addition, $r_j^{(0,\pm1)}$ in Eq. 2.7 are also expressed in terms of $i\xi$ and $k_\perp$ as follows:

$$r_{TM}^{(0,\pm1)}(i\xi,k_\perp) = \frac{\varepsilon_{\pm1}(i\xi)k_0(i\xi,k_\perp) - \varepsilon_0(i\xi)k_{\pm1}(i\xi,k_\perp)}{\varepsilon_{\pm1}(i\xi)k_0(i\xi,k_\perp) + \varepsilon_0(i\xi)k_{\pm1}(i\xi,k_\perp)} \tag{2.10}$$

$$r_{TE}^{(0,\pm 1)}(i\xi, k_\perp) = \frac{k_0(i\xi, k_\perp) - k_{\pm 1}(i\xi, k_\perp)}{k_0(i\xi, k_\perp) + k_{\pm 1}(i\xi, k_\perp)} \tag{2.11}$$

Up to now, F_{C-L} expression are valid T = 0 K. In that case, the only contribution to the fluctuations of the EM field are due to the zero-point energy. At a finite temperature $T > 0$ K, thermal fluctuations of the EM field also contribute to the Casimir-Lifshitz force. In what follows, it will be shown how to calculate F_{C-L} at any temperature $T \geq 0$ K. Note that, although the dielectric function of materials may be affected by temperature changes, for the materials and temperatures considered in this thesis, variations with T will be negligible. Therefore, dielectric functions will be considered unaltered under temperature changes.

According to Bose-Einstein statistics, the population of an EM field mode of frequency ω at finite temperature T is:

$$p(\omega) = \frac{1}{2} + \frac{1}{e^{\hbar\omega/k_bT} - 1} = \frac{1}{2} coth \frac{\hbar\omega}{2k_BT} \tag{2.12}$$

where the 1/2 term is associated to zero-point fluctuations, and $\frac{1}{e^{\hbar\omega/k_bT}-1}$ to thermal fluctuations. Taking all this into account, the expression of the Casimir-Lifshitz force at finite temperature expressed in real frequencies can be rewritten as:

$$F_{C-L}\,(d_0, T) = -\frac{\hbar}{2\pi^2} \int_0^\infty k_\perp \, dk_\perp \int_0^\infty d\omega coth \frac{\hbar\omega}{2k_BT}$$
$$Im \left\{ k_0 \sum_{j=TE,TM} \left[\frac{e^{2k_0 d_0}}{r_j^{(0,1)}(\omega, k_\perp) \cdot r_j^{(0,-1)}(\omega, k_\perp)} - 1 \right]^{-1} \right\} \tag{2.13}$$

This expression is equivalent to that given in Eq. 2.1. Again, F_{C-L}

depends exponentially on $k_{l=0}$, and so, rapid oscillations are included in the integrand. They can be eliminated by performing the integral in the complex plane of frequencies Ω, as it was shown in Eq. 2.6. However, in this case, the function $coth\frac{\hbar\Omega}{2k_BT}$ in the integrand introduces an infinite number of poles for $\Omega = i\xi_m$, with ξ_m defined as:

$$\xi_m = \frac{2\pi k_B T}{\hbar} \cdot m \tag{2.14}$$

being m = 0, 1, 2,... ∞. These discrete ξ_m frequencies are commonly named *Matsubara frequencies*. The fact of having those poles in the imaginary axis (showed as points in Fig. 2.2(b)) leads to the calculation of residues to compute the integral along the straight segment L_2. Because of that, the integral in frequencies ω in Eq. 2.13 is replaced by a summatory over Matsubara frequencies $i\xi_m$. Explicitly, the modification in the expression is:

$$\frac{\hbar}{2\pi}\int_0^\infty d\xi \longleftrightarrow k_B T \sum_{m=0}^{\infty}{}' \tag{2.15}$$

where the prime (') indicates that the term with $m = 0$ is multiplied by 1/2. This substitution gives rise to the expression of F_{C-L} at $T > 0$ K:

$$F_{C-L}\left(d_0, T\right) = -\frac{k_B T}{\pi} \sum_{m=0}^{\infty}{}' \int_0^\infty k_0^m k_\perp \, dk_\perp \cdot$$
$$\cdot \sum_{j=TE,TM} \left[\frac{e^{2k_0^m d_0}}{r_j^{(0,1)}(i\xi_m, k_\perp) \cdot r_j^{(0,-1)}(i\xi_m, k_\perp)} - 1 \right]^{-1} \tag{2.16}$$

with

$$k_l^m = k_l(i\xi_m, k_\perp) = \left[k_\perp^2 + \varepsilon_l(i\xi_m)\frac{\xi_m^2}{c^2}\right]^{1/2} \tag{2.17}$$

In these expressions, the simple Fresnel coefficients $r_j^{(0,1)}(i\xi_m, k_\perp)$ and $r_j^{(0,-1)}(i\xi_m, k_\perp)$ evaluated at the specific frequency $i\xi_m$, given in Eqs. 2.17, 2.10, and 2.11 also apply here.

2.1.2 Systems with arbitrary number of layers

Diverse physical situations in which Casimir-Lifshitz forces play an important role involve systems comprising several materials, and sometimes, these materials can be considered to be built in layers. The expressions for F_{C-L} presented in previous sections can be generalized [98, 99, 100] to systems with an arbitrary number of layers, each one labeled with l = $-L, ..., L$ (L = 1, 2, ...∞), and with the total number of layers given by $2L$+1. Layers are symmetrically piled up above (positive subscripts) and below (negative subscripts) the central material (l=0), which is the one that mediates the interaction between top layers and bottom layers (see scheme in Fig. 2.3). Each layer is described by its dielectric function ε_l, density ρ_l, and thickness d_l, being d_{L+1} and d_{-L-1} equal to infinite as they account for semi-infinite materials. In this configuration, the reflection coefficients on the top and bottom interfaces of layer l=0, now named multiple Fresnel coefficients $R_j^{(+)}$ and $R_j^{(-)}$, respectively, are expressed as an iterative function of the corresponding simple Fresnel reflection coefficients of the interfaces above and below such material. The new generalized expression of F_{C-L} at a finite temperature is written as:

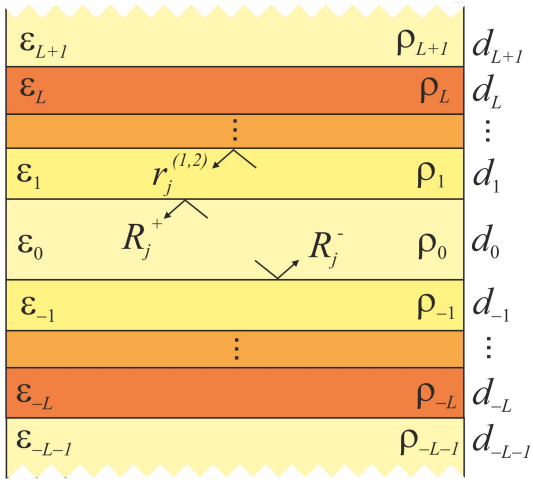

Figure 2.3: Scheme of a mutilayer structure of an arbitrary number of layers for the F_{C-L} calculation. Each layer is characterized by its dielectric function ε_l, density ρ_l and thickness d_l, where layer with $l = 0$ stands for the material mediating the interaction between top layers and bottom layers. $R_j^{\pm}$ are the multiple Fresnel coefficients on the top (+) and the bottom (-) interfaces of the material mediating the interaction.

$$F_{C-L}\left(d_0,T\right)=-\frac{k_BT}{\pi}\sum_{m=0}^{\infty}{}'\int_0^{\infty}k_0^m k_\perp dk_\perp\cdot\sum_{j=TE,TM}\left[\frac{e^{2k_0^m d_0}}{R_j^{(+)}\cdot R_j^{(-)}}-1\right]^{-1} \tag{2.18}$$

with $R_j^{(\pm)}$ defined as:

$$R_j^{(\pm)}(m,k_\perp)=\Gamma_{l=0}^{(\pm)}(m,k_\perp) \tag{2.19}$$

and the $\Gamma_l^{(\pm)}$ functions expressed as:

$$\Gamma_l^{(\pm)}(m,k_\perp)=\frac{r_j^{(l,l\pm1)}+\Gamma_{l\pm1}e^{-2k_{l\pm1}^m d_{l\pm1}}}{1+r_j^{(l,l\pm1)}\Gamma_{l\pm1}e^{-2k_{l\pm1}^m d_{l\pm1}}} \tag{2.20}$$

2.1.3 Dielectric function of materials

The dielectric function of a material, $\varepsilon(\omega)$, is a magnitude that describes the response of a material to an external EM field of frequency ω. In particular, it is the factor that relates the electric displacement field ($\overrightarrow{D}$) with the applied electric field ($\overrightarrow{E}$):

$$\overrightarrow{D}=\varepsilon\overrightarrow{E}=\epsilon_0\varepsilon\overrightarrow{E}=\epsilon_0\overrightarrow{E}+\overrightarrow{P} \tag{2.21}$$

being ϵ_0 the vacuum permittivity, ε the relative permittivity or dielectric function, and $\overrightarrow{P}$ the polarization density.

As the materials response to an external EM field is not instantaneous and it obeys a causal process described by the Kramers-Kronig relations, the dielectric function is expressed as a complex function, $\varepsilon(\omega)=\varepsilon'(\omega)-i\varepsilon''(\omega)$, in order to specify the magnitude and the phase difference

between $\overrightarrow{D}$ and $\overrightarrow{E}$.

It is important to note that the dielectric function and the refractive index of a material are related through the relation $\varepsilon = \tilde{n}^2$ with $\tilde{n} = n - ik$, so that $\varepsilon' = n^2 - k^2$, and $\varepsilon'' = 2nk$. The imaginary part of $\tilde{n}$, k is named extinction coefficient and it accounts for the specific absorption loss of the material.

The dielectric function is an inherent material property, and it has been demonstrated its strong dependence on the sample preparation process [101, 102]. The dielectric function can be experimentally measured employing different techniques, and the technique to be applied will depend on the frequency range of interest. Additionally, it can also be modeled from limited tabulated experimental data by using a simple oscillator models [103, 104, 105]. They are based on the equation of motion of classical electrons harmonically bounded to atoms interacting with an electric field, resulting in a sum of absorption peaks with a Gaussian or Lorentzian shape. These models were originally used when dealing with dispersion forces because dielectric data at vacuum ultraviolet ranges were not able to be measured or were not precisely known. Only recently, accurate measurements have been achieved.

In Lifshitz theory, which solves the microscopic Maxwell's equations, the dielectric function enters directly in the formalism, playing a central role as it is the term which contains the information about the interacting materials.

As it was pointed out in the previous section, Lifshitz theory is much simpler to compute considering the complex plane of frequencies than the real axis. Because of that, also the dielectric function evaluated at imaginary frequencies using Eq. 2.9 should be employed in order to simplify the calculation of F_{C-L}.

Figure 2.4 illustrates examples of how the dielectric function changes when real frequencies ω (panel (a)) rotate to imaginary frequencies $i\xi$ (panel (b)), for SiO_2 (orange line) and PS (light blue line) materials. Their

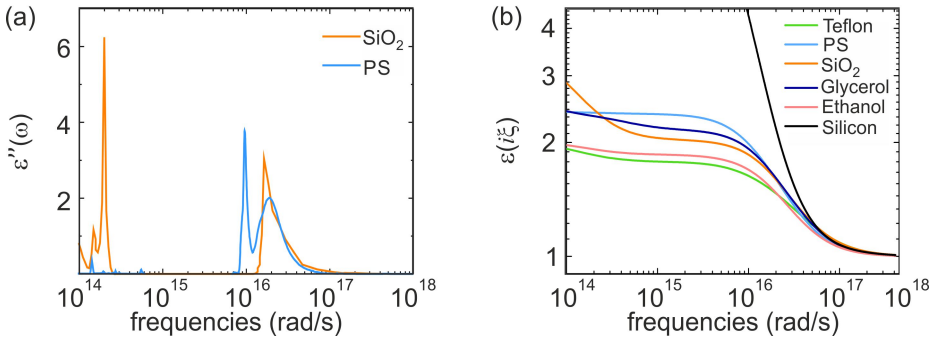

Figure 2.4: (a) Dielectric function of SiO_2 (orange) and PS (blue) at real frequencies and (b) dielectric function evaluated at Matsubara frequencies for several materials.

tabulated dielectric data in real frequencies are found in references [106, 107, 108, 109]. In addition, in panel (b) dielectric functions evaluated directly at Matsubara frequencies are also shown for some other reported materials [105]. In Fig. 2.5 it is shown the extinction coefficient k (panel (a)), and the dielectric function evaluated at Matsubara frequencies $\epsilon(i\xi)$ (panel (b)) of SiO_2, as a function of the angular frequencies. High k values, which account for high absorption of the material, correspond to high negative slopes of $\varepsilon(i\xi)$. In the figure, such behaviour is observed in the UV and the IR frequency ranges, i.e., from 10^{13} to 10^{15} rad·s^{-1}, and from 10^{16} to 10^{17} rad·s^{-1}. On the contrary, transparent frequency ranges with $k \approx 0$, correspond to zero slope regions in the $\varepsilon(i\xi)$ curve.

As it was mentioned in previous sections, the nature and intensity of the Casimir-Lifshitz force strongly depend on the dielectric function of the materials involved and their relation to one another. Some predictions on the attractive or repulsive nature of F_{C-L} might be established when comparing the dielectric functions in Matsubara frequencies before performing full calculations.

Along this thesis, one of the main goals will be to find materials combinations displaying repulsive Casimir-Lifshitz forces. To this end, the

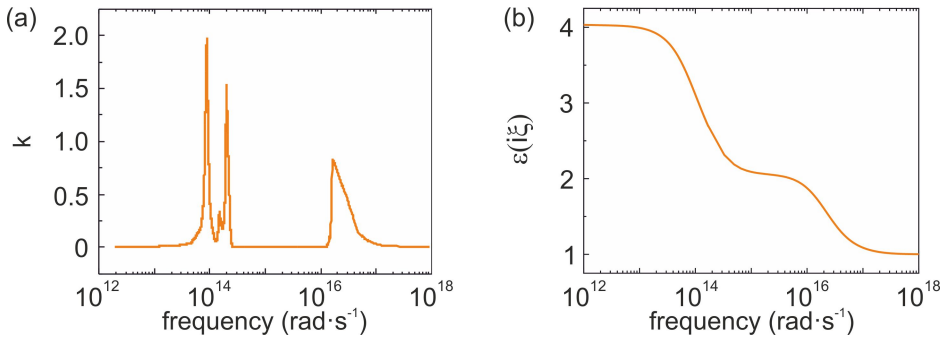

Figure 2.5: (a) Imaginary part of the refractive index, k and (b) dielectric function evaluated at the Matsubara frequencies $\varepsilon(i\xi)$ for SiO_2.

comparative relation expressed in Eqs. 1.3 and 1.4 for the dielectric functions of the materials in the system will be pursued.

2.1.4 Semi-analytical calculations

Concerning the computation of F_{C-L}, results reported by Elbaum and Schick in 1990 [110] will be first reproduced. In their study, it is shown how the Casimir-Lifshitz force would promote the growth of water as a nanometer thick layer above an ice surface in air at $T = 273.15$ K. Three materials compose the multilayer scheme, and F_{C-L} can be estimated through Eqs. 2.16 for 3 materials, or 2.18 for a generalized multilayer structure. In the latter case, L would be equal to 1. Both expressions present an integral in $k_\perp$ from 0 to ∞ and a summatory over the Matsubara frequencies. Therefore, the convergence of the integrand must be ensured for the upper limits of the integrals over ξ_m and $k_\perp$, for the range of separation distances considered. In Fig. 2.6(a), materials labeled as l = 1, 0, -1 will correspond to air, water and ice, respectively. The values of the dielectric functions for those materials are the same used in Elbaum and Schick's paper and they are shown in Fig. 2.6(b).

Figure 2.7(a) shows, on the one hand, an example of one integrand as

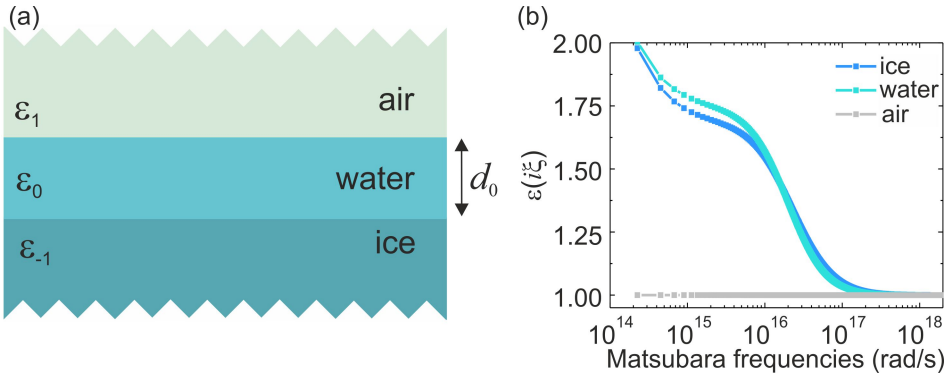

Figure 2.6: (a) Scheme of the three materials system consisting in a d_0 thick layer of water in between semi-infinite air and ice slabs. (b) Dielectric function of the three materials evaluated at Matsubara frequencies extracted from Ref. [110]

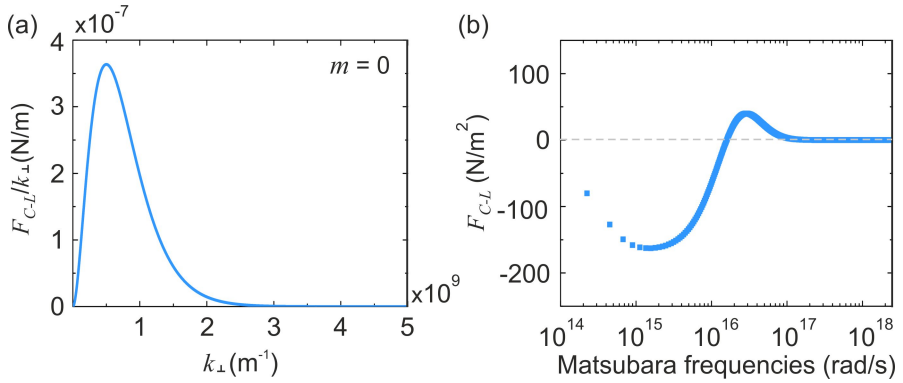

Figure 2.7: (a) Integrand of F_{C-L} in Eq. 2.16 as a function of $k_\perp$ for $m = 0$ and d_0 = 2 nm. (b) Contribution of each Matsubara frequency to F_{C-L}. These contributions correspond to each term in the summatory in Eq. 2.16, evaluating m = [1-10,000]. For m = 0 the contribution is 672 N/m². Positive and negative values will produce repulsive and attractive contributions, correspondingly.

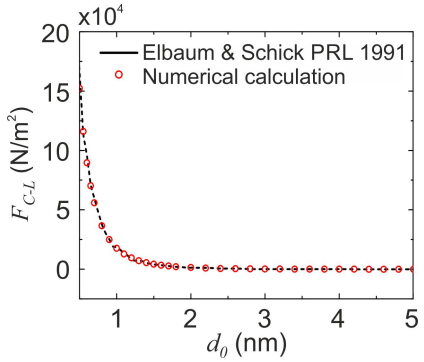

Figure 2.8: F_{C-L} as a function of d_0 for the system considered in Fig. 2.6(a). Black solid line represents the resulting F_{C-L} from Ref. [110], whereas red circles display the numerical calculation carried out applying Eq. 2.16.

a function of $k_\perp$ for a given Matsubara frequency. The frequency selected is the first m value defining Matsubara frequencies, i.e., m = 0, which represents the largest contribution to F_{C-L}. Calculations are performed for an arbitrary separation distance of d_0 = 2 nm. As it can be observed, the integrand converges at large $k_\perp$ values, using steps of 10^4 m^{-1}. On the other hand, panel (b) displays, as a function of Matsubara frequencies, the discrete values obtained after the integration of the curves equivalent to the one shown in panel (a), but for all m values, i.e., for m = 0, 1, ... ∞. Note that the contribution of m = 0 is 672 N/m^2, a value not shown in panel (b) due to the logarithmic scale. For large Matsubara frequencies (as large as that given for $m = 10^4$), the curve in panel (b) decays to zero. The final F_{C-L} value will be the summatory of all discrete points in panel (b). In this case, F_{C-L} is 1347 N/m^2 at d_0 = 2 nm.

Original results in Ref. [110] are expressed in energy instead of force. For comparison, those results have been here transformed to force values and are shown in Fig. 2.8 for separation distances d_0 = [1-4] nm. Recall that both energy and force magnitudes are given per unit area. Reproduc-

tion of results is excellent. Once this example, and others in literature including metals [101, 111] were reproduced, novel designs were explored.

As an aside, to give an idea of the computational cost to perform this kind of integrals, it was checked that the calculation of F_{C-L} for three layers at a given separation distance takes around 30 seconds in a computer with an Intel Core i7 processor.

2.2 Electrostatic force

Together with F_{C-L}, the electrostatic force, F_{el}, is a dominant force at micro- and nanoscales. In fact, the electrostatic force between two metallic plates separated d = 1 μm with a potential difference of V = 17 mV, give rises to a coulomb interaction in the same order of magnitude as F_{C-L}. Because of that, F_{el} must be taken into account when analyzing forces at the nanoscale, and generally, it should be eliminated in order to be able to measure experimentally F_{C-L}. In the particular case of a fluid material mediating the interaction, which is the typical scenario addressed in this thesis, in the plane-parallel geometry the electrostatic interaction yields to the double-layer force, F_{dl}. This force appears when two surfaces present surface charge (σ_β with β = 1,2 for each surface) and ions of opposite electric sign dissolved in the fluid are attracted by coulombic interaction. As a result, a layer of opposite charge is deposited near the surfaces (see Fig. 2.9). The characteristic thickness of the ions deposited layer is related to the Debye length, l_D, defined as the inverse of the Debye screening wave vector K_D, which is related to the distance at which the electrical potential decreases a factor 1/e. To calculate the double-layer force between the two surfaces with their respective ions layers, the Poisson-Boltzmann approximation is used to describe the electrostatic potential, and the double-layer force per unit area is obtained from it in the

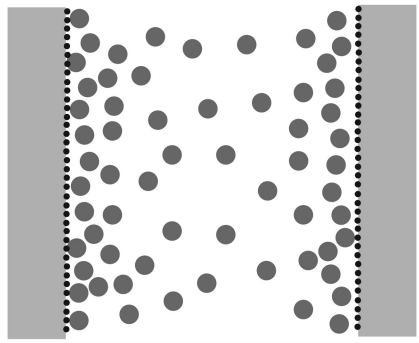

Figure 2.9: Scheme of the charge distribution between two plates separated by a fluid. Ions attache to the surface and counterions distribute following a Boltzmann distribution.

limit of small potentials [112, 113].

$$F_{dl} = \frac{2}{\varepsilon\varepsilon_0} \frac{\sigma_1^2 + \sigma_2^2 + \sigma_1\sigma_2(e^{K_D d_0} + e^{-K_D d_0})}{(e^{K_D d_0} - e^{-K_D d_0})^2} \tag{2.22}$$

In the above expression, d_0 is the separation distance between the surfaces, ε the dielectric function of the fluid, and K_D is the inverse of the Debye length l_D defined as:

$$K_D = \frac{1}{l_D} = \sqrt{\frac{2(Ze)^2 N}{\varepsilon k_B T}} \tag{2.23}$$

with e the electron charge, and N and Z the number per unit volume and the valence of the salt ions, respectively.

2.3 Roughness and patch potentials effect

Experimentally, samples are not perfect and the synthesis or fabrication process may affect their properties making them unique. Apart from the

optical properties mentioned in the previous section, a deep analysis in literature regarding the effect of roughness and patch potentials in experimental measurements of F_{C-L} have been performed, showing that the effect of both type of imperfections on F_{C-L} depend on the fabrication procedure.

On the one hand, regarding the roughness of surfaces, many efforts were put on its analytical description and the quantification of its effect on F_{C-L} [114, 115, 116, 117, 111, 118, 119, 120]. All those methods are based on the knowledge of the height profile of the two bodies interacting, that is the self-affine roughness of each surface. Typically, that profile is experimentally measured using an atomic force microscope giving a precise map of the topology of the sample. Using such information as input some works apply a method that extract statistical parameters based on a model for the height-height correlation of self-affine roughness [117, 119], other works employ perturbation theory in order to estimate the roughness correction to F_{C-L} [114, 116, 115], and the most detailed method [120] separates the problem into two regimes: heights smaller and larger compared to the root-mean-square of height fluctuations of the surface. Basically, the roughness correction to the F_{C-L} is given by three contributions $F_{C-L} = F_{PT} + F_{PFA}$, the perturbation term F_{PT} that describes the effect of roughness comparable to the root-mean-square and the last two terms corresponding to high peaks and deep troughs estimated by the proximity force approximation. Finally it is found that roughness corrections become significant at separation distances below 100 nm [119], attaining modest corrections such as 0.65% or 0.42% for two gold coated plates interacting, with maximum heights of the roughness peaks smaller than 25nm, separated 160 and 200 nm, respectively [111].

On the other hand, apart from the electrostatic force due to the residual potential difference between the interacting bodies, it is possible to find a spatial variation of the surface potential in the sample caused by the grains of the polycrystalline material. This spatial distribution of surface

potential is named *patch potentials* and may cause discrepancies among experimental measurements of F_{C-L} and the theory. Again analytical models have been developed to quantify that electrostatic force [121] and its effect on F_{C-L} measurements [122, 123]. In this case the experimental information about the spatial distribution of patch potential is determined through Kelvin Probe microscopy, which consists on contactless measurements of the electrostatic interaction between a cantilever and a sample [124, 123]. For typical patch sizes around 200 nm, the electrostatic force associated to the patch potentials between two golden coated plates interacting at separation distance of 160 nm is a 0.037% compared to F_{C-L} and becoming even smaller at larger separation distance.

In the following, in this thesis the effect of roughness and patch potential will be neglected since their effect have been proven to be very small in the range of hundred of nanometers which is the typical values of the separation distances here studied and in order to focus the analysis on the effect of the optical properties of materials involved in the Casimir-Lifshitz interaction.

2.4 Transfer Matrix Method

To analyse the optical properties of the systems under study, the Transfer Matrix Method (TMM) will be used [125]. The TMM provides an analytical description of the propagation of EM fields through isotropic stratified materials. The method, based on the boundary conditions at the interfaces between materials, solves the amplitude of the EM field at each point of space. Specifically, along this thesis, the TMM is used to simulate the optical response of multilayer plane-parallel systems in terms of the reflectance (R), absorptance (A), transmittance (T), and the spectral and spatial distribution of the EM field and the power absorbed.

Let us consider a multilayer structure made up of L layers as the one shown in Fig. 2.10, where n_l and d_l are, respectively, the complex refrac-

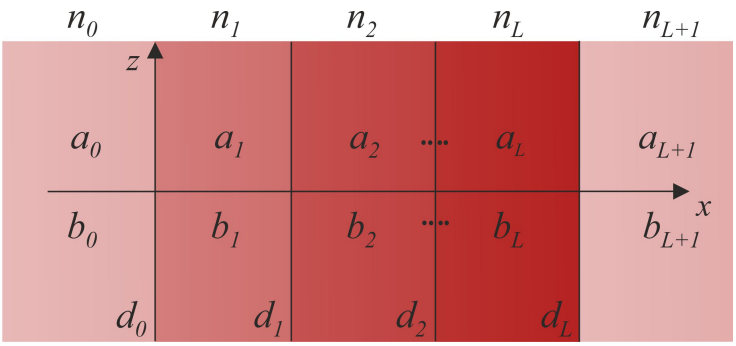

Figure 2.10: Scheme of a multilayer structure with N layers.

tive index and the layer thickness. Subscript 0 and $L+1$ stand for semi-infinite materials enclosing the multilayer structure. Inside the structure, the EM field propagates along the x-axis, with the electric field (E) oscillating either in the xy plane, named transverse electric mode (TE), or in the xz plane, named transverse magnetic mode (TM).

At each point of space, E can be described by Eq. 2.24 which is based on the superposition of two monochromatic plane waves travelling in opposite direction.

$$E = E(x)e^{i(\omega t - \beta z)} \equiv a(x)e^{-ik_x x} + b(x)e^{ik_x x} \tag{2.24}$$

In the above equation, a and b are the amplitude of the wave propagating rightwards and leftwards, correspondingly, while β and k_x are the z- and x-component of the wavenumber k, respectively. Applying Eq. 2.24 to the stratified structure results in a system of $L+2$ equations (Eq. 2.25):

$$E(x) = \begin{cases} a_0 e^{-ik_{0x}(x-d_0)} + b_0 e^{ik_{0x}(x-d_0)}, & x < d_0 \\ a_l e^{-ik_{lx}(x-d_{l-1})} + b_l e^{ik_{lx}(x-d_{l-1})}, & d_{l-1} < x < d_l \\ a_L e^{-ik_{Lx}(x-d_L)} + b_L e^{ik_{Lx}(x-d_L)}, & x > d_L \end{cases} \tag{2.25}$$

where a_l and b_l are the coefficients of the EM field inside each homogeneous layer and k_{lx} is the x-component of k, which is constant inside each layer and is defined as:

$$k_{lx} = n_l \frac{\omega}{c} cos(\theta_l) \tag{2.26}$$

with θ_l the incident angle of radiation with respect to the x-axis in layer l.

The system of equations can be written in a more compact notation using products of matrices. Thus, at an interface between two materials, the amplitudes on the left-side (a_l,b_l) and right-side (a_{l+1}, b_{l+1}) are related through the dynamical matrix (D).

$$\begin{pmatrix} a_l \\ b_l \end{pmatrix} = D_l^{-1} D_{l+1} \begin{pmatrix} a_{l+1} \\ b_{l+1} \end{pmatrix} \tag{2.27}$$

D_l appearing in the above expression is defined next in Eq. 2.28 and Eq. 2.29 for TE and TM polarizations, correspondingly.

$$D_l = \begin{pmatrix} 1 & 1 \\ n_l cos(\theta_l) & -n_l cos(\theta_l) \end{pmatrix} \tag{2.28}$$

$$D_l = \begin{pmatrix} cos(\theta_l) & cos(\theta_l) \\ n_l & -n_l \end{pmatrix} \tag{2.29}$$

The product $D_l^{-1} D_{l+1}$ represents the transmission matrix between material layers l and $l+1$, and the propagation of light inside the layer until the next interface is described by matrix P.

$$\begin{pmatrix} a_l \\ b_l \end{pmatrix} = P_l D_l^{-1} D_{l+1} \begin{pmatrix} a_{l+1} \\ b_{l+1} \end{pmatrix} \tag{2.30}$$

with

$$P_l = \begin{pmatrix} e^{i\phi_l} & 0 \\ 0 & e^{-i\phi_l} \end{pmatrix} \tag{2.31}$$

being ϕ_l the phase at the interface $x = d_l$ between layer l and $l+1$

$$\phi_l = k_{lx} \cdot d_l \tag{2.32}$$

Therefore, each layer in the system introduces two interfaces, being the propagation of light through each layer expressed by $D_l P_l D_l^{-1}$. The subsequent product of matrices for the whole structure can be rewritten as an unique matrix with elements M_{ij}, relating amplitudes from both sides of the stratified media as it shows Eq. 2.33 and 2.34.

$$\begin{pmatrix} a_0 \\ b_0 \end{pmatrix} = \begin{pmatrix} M_{11} & M_{12} \\ M_{21} & M_{22} \end{pmatrix} \begin{pmatrix} a_{L+1} \\ b_{L+1} \end{pmatrix} \tag{2.33}$$

$$\begin{pmatrix} M_{11} & M_{12} \\ M_{21} & M_{22} \end{pmatrix} = D_0^{-1} \left[\prod_{l=1}^{L} D_l P_l D_l^{-1} \right] D_{L+1} \tag{2.34}$$

From the matrix elements M_{ij}, one can extract information about the optical response of the whole stratified system knowing which fraction of the incident radiation is reflected R or transmitted T.

$$R = |r|^2 = \left| \frac{M_{21}}{M_{11}} \right|^2 \tag{2.35}$$

$$T = \frac{n' cos(\theta')}{n_0 cos(\theta_0)} |t|^2 = \frac{n' cos(\theta')}{n_0 cos(\theta_0)} \left| \frac{1}{M_{11}} \right|^2 \tag{2.36}$$

From conservation of energy, light that is not reflected nor transmitted must be absorbed by the subsequent layers. Thus, the absorption of the

system can be expressed as

$$A = 1 - R - T \tag{2.37}$$

2.5 Field distribution and power absorbed

In order to gain physical insight into the light-matter interaction, the spatial distribution of the electric field intensity ($|E(\omega, r)|^2$) across materials, and the optical power absorbed (P_{abs}) by each slab is inspected for stratified structures in this thesis.

First, the spatial and spectral distribution of the electric field intensity is obtained using the TMM described in the previous section. After that, the spatial and spectral optical power absorbed by the material is extracted by using the following expression:

$$P_{Abs}(\omega) = \frac{1}{2} \int_0^V \omega \epsilon_0 \varepsilon_l''(\omega, \mathbf{r}) |E(\omega, \mathbf{r})|^2 \, dV \tag{2.38}$$

where $\varepsilon_l''(\omega)$ is the imaginary part of the dielectric function of the material in layer l, and V is the total volume occupied by the whole stratified structure.

Generally, the absorptance (A) of any system can be seen as the fraction of the incident power (P_0) that has been absorbed.

$$A = \frac{P_{Abs}}{P_0} \tag{2.39}$$

being possible to separate the absorptance in each layer from the total A by computing the path integral of the power absorbed per unit volume (δA) between the corresponding limits of each layer. At normal incidence and being z the perpendicular axis to the slab surface, the absorptance is

given by:

$$A = \int \delta A \, dz \tag{2.40}$$

In Chapter 5 it will be shown that this information sheds light into results that, otherwise, could not be retrieved experimentally. For the moment, as an example, Fig. 2.11 illustrates the kind of analysis to be performed by means of the TMM. In it, as it is depicted in panel (a), a stratified thin film comprising four layers of 10 nm thick, two made of silicon dioxide (SiO_2) (in orange) and two made of polystyrene (PS) (in blue), are considered. Results for the spatial and spectral $|E|^2$ and δA distributions are shown in panels (b) and (c), respectively, and the spectral power absorbed in regions or layers denoted as I, II, III and IV are displayed in (d). Regions I and III correspond to SiO_2 layers and II and IV to PS slabs. Notice that in panels (b) and (c) light is considered to propagate from the bottom (negative values of position) to the top (positive values of position) of the panel. To guide the eye, white horizontal lines mark the limits of each layer. As it will be discussed in Chapter 5, materials only absorb light at wavelengths in which $\varepsilon_l''(\omega) \neq 0$ and $|E|^2$ is sufficiently intense, resulting in the film absorptance (black line in pannel (d)) as the summatory of the power absorbed by each layer (colored lines in pannel (d)).

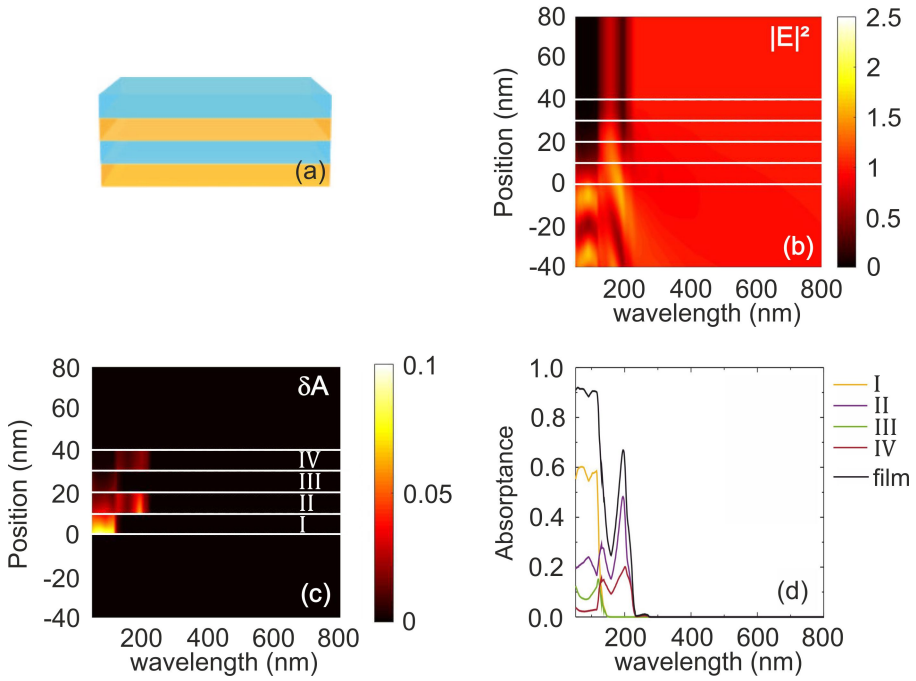

Figure 2.11: (a) Scheme of the 40 nm thick thin film consisting in two layers of SiO_2 (orange) and two layers of PS (blue) interleaved. (b) Spectral and spatial electric field intensity $|E|^2$ distribution. White horizontal lines delimit layer interfaces. (c) Spectral and spatial power absorbed per unit volume. Labels I, II, III, IV stand for the four regions of space occupied by material layers. (d) Spectral absorptance of each region of space (colored lines) and spectral total absorptance of the thin film (black line).

Chapter 3

Levitation of thin films due to Casimir-Lifshitz interactions. Analysis of temperature effects

The results of this chapter are gathered and published in the following reference:

V. Esteso, S. Carretero-Palacios, and H. Míguez. **Effect of temperature variations on equilibrium distances in levitating parallel dielectric plates interacting through Casimir forces**. *Journal of Applied Physics*, 119(14), 144301, 2016.

3.1 Introduction

3.2 Levitation Phenomena in plane-parallel systems due to Casimir-Lifshitz and gravity force balance

3.3 Temperature dependence of equilibrium distance at room temperature

3.4 Simple rules to predict temperature variation effects on d_{eq}

3.5 Conclusions

Chapter 4

Optical resonators based on Casimir-Lifshitz forces

The results of this chapter are gathered and published in the following reference:

V. Esteso, S. Carretero-Palacios, and H. Míguez. **Casimir-Lifshitz Force Based Optical Resonators**. *The Journal of Physical Chemistry Letters*, 10(19), 5856-5860, 2019.

4.1 Introduction

4.2 Fabry-Pérot optical cavities

4.3 CasimirLifshitz Force Based Optical Resonators

4.4 High Q-factor optical resonators for accurate measurements of repulsive F_{C-L}

4.5 Effect of room temperature variations on the force balance and the optical cavity characterization

4.6 Conclusions

Chapter 5

Optical Interference Effects on Casimir-Lifshitz Forces

The results of this chapter are gathered and published in the following reference: V. Esteso, S. Carretero-Palacios, and H. Míguez. **Optical interference effects on the Casimir-Lifshitz force in multilayer structures**. *Physical Review A*, 101(3), 033815, 2020.

5.1 Introduction

5.2 Periodic multilayer structures and their optical response

5.3 Effect of thickness and number of layers on Casimir-Lifshitz force

5.4 Tuning the Casimir-Lifshitz force with multilayer nanostructures

5.5 Conclusions

Bibliography

[1] Kellar Autumn, Metin Sitti, Yiching A Liang, Anne M Peattie, Wendy R Hansen, Simon Sponberg, Thomas W Kenny, Ronald Fearing, Jacob N Israelachvili, and Robert J Full. Evidence for van der waals adhesion in gecko setae. *Proceedings of the National Academy of Sciences*, 99(19):12252–12256, 2002. 1

[2] Zhao Yapu. Stiction and anti-stiction in mems and nems. *Acta Mechanica Sinica*, 19(1):1–10, 2003. 1

[3] Frank W DelRio, Maarten P de Boer, James A Knapp, E David Reedy Jr, Peggy J Clews, and Martin L Dunn. The role of van der waals forces in adhesion of micromachined surfaces. *Nature materials*, 4(8):629, 2005. 1, 12

[4] Roland Schmid. Recent advances in the description of the structure of water, the hydrophobic effect, and the like-dissolves-like rule. *Monatshefte für Chemie/Chemical Monthly*, 132(11):1295–1326, 2001. 1

[5] CW Ormel, M Spaans, and AGGM Tielens. Dust coagulation in protoplanetary disks: porosity matters. *Astronomy & Astrophysics*, 461(1):215–232, 2007. 1

[6] Peter W Milonni. *The quantum vacuum: an introduction to quantum electrodynamics*. Academic press, 2013. 1, 5, 9

[7] Stefan Yoshi Buhmann. *Dispersion Forces I: Macroscopic quantum electrodynamics and ground-state Casimir, Casimir–Polder and van der Waals forces*, volume 247. Springer, 2013. 1

[8] Mathias Boström, David RM Williams, and Barry W Ninham. Surface tension of electrolytes: specific ion effects explained by dispersion forces. *Langmuir*, 17(15):4475–4478, 2001. 1

[9] Jacob N Israelachvili. van der waals dispersion force contribution to works of adhesion and contact angles on the basis of macroscopic theory. *Journal of the Chemical Society, Faraday Transactions 2: Molecular and Chemical Physics*, 69:1729–1738, 1973. 1

[10] János Ángyán, John Dobson, Georg Jansen, and Tim Gould. *London Dispersion Forces in Molecules, Solids and Nano-structures: An Introduction to Physical Models and Computational Methods*. Royal Society of Chemistry, 2020. 1

[11] B Silver. *The physical chemistry of membranes: an introduction to the structure and dynamics of biological membranes*. Springer Science & Business Media, 2012. 1

[12] Ali Chami Khazraji and Sylvain Robert. Self-assembly and intermolecular forces when cellulose and water interact using molecular modeling. *Journal of Nanomaterials*, 2013, 2013. 1

[13] Ken A Dill. Dominant forces in protein folding. *Biochemistry*, 29 (31):7133–7155, 1990. 1

[14] Charles M Roth, Brian L Neal, and Abraham M Lenhoff. Van der waals interactions involving proteins. *Biophysical journal*, 70(2): 977–987, 1996. 1

[15] C Nick Pace, J Martin Scholtz, and Gerald R Grimsley. Forces stabilizing proteins. *FEBS letters*, 588(14):2177–2184, 2014. 1

[16] F Michael Serry, Dirk Walliser, and G Jordan Maclay. The role of the casimir effect in the static deflection and stiction of membrane strips in microelectromechanical systems (mems). *Journal of Applied Physics*, 84(5):2501–2506, 1998. 1, 2

[17] Jian-Gang Guo and Ya-Pu Zhao. Influence of van der waals and casimir forces on electrostatic torsional actuators. *Journal of Microelectromechanical systems*, 13(6):1027–1035, 2004. 1

[18] Wen-Hui Lin and Ya-Pu Zhao. Nonlinear behavior for nanoscale electrostatic actuators with casimir force. *Chaos, Solitons & Fractals*, 23(5):1777–1785, 2005. 1

[19] Fabrizio Pinto. The economics of van der waals force engineering. In *AIP Conference Proceedings*, volume 969, pages 959–968. American Institute of Physics, 2008. 1

[20] George Palasantzas, Mehdi Sedighi, and Vitaly B Svetovoy. Applications of casimir forces: Nanoscale actuation and adhesion. *Applied Physics Letters*, 117(12):120501, 2020. 1

[21] H. B. G. Casimir. On the Attraction Between Two Perfectly Conducting Plates. *Indag. Math.*, 10:261–263, 1948. [Kon. Ned. Akad. Wetensch. Proc.100N3-4,61(1997)]. 2, 6

[22] Y Srivastava, A Widom, and MH Friedman. Microchips as precision quantum-electrodynamic probes. *Physical review letters*, 55 (21):2246, 1985. 2

[23] E Buks and ML Roukes. Stiction, adhesion energy, and the casimir effect in micromechanical systems. *Physical Review B*, 63(3): 033402, 2001. 2

[24] W-H Lin and Y-P Zhao. Casimir effect on the pull-in parameters of nanometer switches. *Microsystem Technologies*, 11(2-3):80–85, 2005. 2

[25] RC Batra, Maurizio Porfiri, and D Spinello. Effects of casimir force on pull-in instability in micromembranes. *EPL (Europhysics Letters)*, 77(2):20010, 2007. 2

[26] David A. T. Somers, Joseph L. Garrett, Kevin J. Palm, and J. N. Munday. Measurement of the casimir torque. *Nature*, 564: 386–389, 2018. 3

[27] Rongkuo Zhao, Lin Li, Sui Yang, Wei Bao, Yang Xia, Paul Ashby, Yuan Wang, and Xiang Zhang. Stable casimir equilibria and quantum trapping. *Science*, 364(6444):984–987, 2019. 3, 13

[28] M. Bordag, G. L. Klimchitskaya, U. Mohideen, and V. M. Mostepanenko. *Advances in the Casimir Effect*. Oxford Science Publications, Oxford, 2009. 5, 21, 24

[29] Fritz London. Z. physik, 1930, 63, 245. *Z. phys. Chem. B*, 11:222, 1930. 5

[30] Hendrik BG Casimir and Dirk Polder. The influence of retardation on the london-van der waals forces. *Physical Review*, 73(4):360, 1948. 6

[31] E. M. Lifshitz. The theory of molecular attractive forces between solids. *Sov. Phys. JETP*, 2:73–83, 1956. 8, 9, 21, 23

[32] IE Dzyaloshinskii, EM Lifshitz, and Lev P Pitaevskii. General theory of van der waals forces. *Soviet Physics Uspekhi*, 4(2):153, 1961. 8, 12

[33] L. H. Ford. Spectrum of the casimir effect and the lifshitz theory. *Physical Review A*, 48(4):2962–2967, 1993. 9

[34] Alejandro Rodriguez, Mihai Ibanescu, Davide Iannuzzi, J. D. Joannopoulos, and Steven G. Johnson. Virtual photons in imaginary time: Computing exact casimir forces via standard numerical electromagnetism techniques. *Phys. Rev. A*, 76:032106, Sep 2007. 9

[35] B. V. Derjaguin, I. I. Abrikosova, and E. M. Lifshitz. Direct measurement of molecular attraction between solids separated by a narrow gap. *Quart. Rev. Chem. Soc.*, 10:295, 1956. 10

[36] Marcus J Sparnaay. Measurements of attractive forces between flat plates. *Physica*, 24(6-10):751–764, 1958. 10

[37] D Tabor and RHS Winterton. Surface forces: Direct measurement of normal and retarded van der waals forces. *Nature*, 219(5159): 1120–1121, 1968. 10

[38] Peter HGM van Blokland and J Theodoor G Overbeek. van der waals forces between objects covered with a chromium layer. *Journal of the Chemical Society, Faraday Transactions 1: Physical Chemistry in Condensed Phases*, 74:2637–2651, 1978. 10

[39] W. Arnold, S. Hunklinger, and K. Dransfeld. Influence of optical absorption on the van der waals interaction between solids. *Phys. Rev. B*, 19:6049–6056, Jun 1979. 10

[40] Steven K Lamoreaux. Demonstration of the casimir force in the 0.6 to 6 μ m range. *Physical Review Letters*, 78(1):5, 1997. 10

[41] Umar Mohideen and Anushree Roy. Precision measurement of the casimir force from 0.1 to 0.9 μ m. *Physical Review Letters*, 81(21): 4549, 1998. 10

[42] RS Decca, D López, E Fischbach, and DE Krause. Measurement of the casimir force between dissimilar metals. *Physical review letters*, 91(5):050402, 2003. 10

[43] H B Chan, Vladimir Aksyuk, R N Kleiman, D J Bishop, and Federico Capasso. Quantum mechanical actuation of microelectromechanical systems by the casimir force. *Science (New York, N.Y.)*, 291:1941–4, 04 2001. 11, 18

[44] AO Sushkov, WJ Kim, DAR Dalvit, and SK Lamoreaux. Observation of the thermal casimir force. *Nature Physics*, 7(3):230–233, 2011. 11

[45] Christopher Hertlein, Laurent Helden, Andrea Gambassi, Siegfried Dietrich, and Clemens Bechinger. Direct measurement of critical casimir forces. *Nature*, 451(7175):172–175, 2008. 11

[46] Jagadishwar Mahanty and Barry W Ninham. *Dispersion forces*, volume 1. Academic Press, 1976. 12

[47] J Israelachvili. Intermolecular and surface forces 2nd edn (new york: Academic). 1992. 12

[48] Roya Maboudian and Roger T Howe. Critical review: Adhesion in surface micromechanical structures. *Journal of Vacuum Science & Technology B: Microelectronics and Nanometer Structures Processing, Measurement, and Phenomena*, 15(1):1–20, 1997. 12

[49] Michael Levin, Alexander P McCauley, Alejandro W Rodriguez, MT Homer Reid, and Steven G Johnson. Casimir repulsion between metallic objects in vacuum. *Physical review letters*, 105(9): 090403, 2010. 12

[50] F. S. S. Rosa, D. A. R. Dalvit, and P. W. Milonni. Casimir-lifshitz theory and metamaterials. *Phys. Rev. Lett.*, 100:183602, May 2008. 12, 18

[51] Direct measurement of repulsive van der waals interactions using an atomic force microscope. *Journal of Colloid and Interface Science*, 180(2):460 – 465, 1996. ISSN 0021-9797. 13

[52] Anders Meurk, Paul F Luckham, and Lennart Bergström. Direct measurement of repulsive and attractive van der waals forces between inorganic materials. *Langmuir*, 13(14):3896–3899, 1997. 13

[53] Seung-woo Lee and Wolfgang M Sigmund. Repulsive van der waals forces for silica and alumina. *Journal of colloid and interface science*, 243(2):365–369, 2001. 13

[54] Seung-woo Lee and Wolfgang M Sigmund. Afm study of repulsive van der waals forces between teflon af™ thin film and silica or alumina. *Colloids and Surfaces A: Physicochemical and Engineering Aspects*, 204(1-3):43–50, 2002. 13

[55] Adam A Feiler, Lennart Bergström, and Mark W Rutland. Superlubricity using repulsive van der waals forces. *Langmuir*, 24(6): 2274–2276, 2008. 13

[56] PJ Van Zwol, Georgios Palasantzas, and J Th M DeHosson. Weak dispersive forces between glass and gold macroscopic surfaces in alcohols. *Physical Review E*, 79(4):041605, 2009. 13

[57] Federico Capasso, Jeremy N Munday, Davide Iannuzzi, and HB Chan. Casimir forces and quantum electrodynamical torques: Physics and nanomechanics. *IEEE Journal of Selected Topics in Quantum Electronics*, 13(2):400–414, 2007. 13

[58] J. N. Munday, F. Capasso, and V. A. Parsegian. Measured long-range repulsive casimir–lifshitz forces. *Nature*, 457:170 – 173, 2009. 13

[59] PJ van Zwol, Georgios Palasantzas, and J Th M De Hosson. Influence of dielectric properties on van der waals/casimir forces in solid-liquid systems. *Physical Review B*, 79(19):195428, 2009. 13

[60] JN Munday, Federico Capasso, V Adrian Parsegian, and Sergey M Bezrukov. Measurements of the casimir-lifshitz force in fluids: The effect of electrostatic forces and debye screening. *Physical Review A*, 78(3):032109, 2008. 13

[61] A. K. Geim and K. S. Novoselov. The rise of graphene. *Nature Materials*, 6(3):183–191, 2007. 17

[62] Harold W Kroto, John E Fischer, and Deann Cox. *The fullerenes*. Newnes, 2012. 17

[63] Lien-Wen Chen and Jia-Yi Yeh. Sonic and photonic crystals. *CRYSTALS*, 10(11):994, 2020. 17

[64] Johnson S. G. Winn J. N. Joannopoulos, J. D. and R. D. Meade. *Photonics Crystals: molding the flow of light*. Princeton University Press, 2008. 17

[65] Boris Isaakovich Shklovskii and Alex L Efros. *Electronic properties of doped semiconductors*, volume 45. Springer Science & Business Media, 2013. 17

[66] Phillip Szuromi and Brent Grocholski. Natural and engineered perovskites. 358(6364):732–733, 2017. 17

[67] Hong Chen, Lin Yuan, Wei Song, Zhongkui Wu, and Dan Li. Biocompatible polymer materials: role of protein–surface interactions. *Progress in Polymer Science*, 33(11):1059–1087, 2008. 17

[68] Lucjan Jacak, Pawel Hawrylak, and Arkadiusz Wojs. *Quantum dots*. Springer Science & Business Media, 2013. 17

[69] Xiaoshan Xu. A brief review of ferroelectric control of magnetoresistance in organic spin valves. *Journal of Materiomics*, 4(1):1–12, 2018. 17

[70] Henry J Snaith. Present status and future prospects of perovskite photovoltaics. *Nature Materials*, 17(5):372–376, 2018. 17

[71] Amir Hossein Rajabi, Michael Jaffe, and Treena Livingston Arinzeh. Piezoelectric materials for tissue regeneration: A review. *Acta biomaterialia*, 24:12–23, 2015. 17

[72] RL Comstock. Review modern magnetic materials in data storage. *Journal of Materials Science: Materials in Electronics*, 13(9):509–523, 2002. 17

[73] Shaobin Wang. Ordered mesoporous materials for drug delivery. *Microporous and mesoporous materials*, 117(1-2):1–9, 2009. 17

[74] RJ Archer. Materials for light emitting diodes. *Journal of Electronic Materials*, 1(1):127–153, 1972. 17

[75] Xiaolong Liu and Mark C Hersam. 2d materials for quantum information science. *Nature Reviews Materials*, 4(10):669–684, 2019. 17

[76] John A Buck. *Fundamentals of optical fibers*, volume 50. John Wiley & Sons, 2004. 17

[77] Allan W Snyder and John Love. *Optical waveguide theory*. Springer Science & Business Media, 2012. 17

[78] Hemant Kumar Raut, V Anand Ganesh, A Sreekumaran Nair, and Seeram Ramakrishna. Anti-reflective coatings: A critical, in-depth review. *Energy & Environmental Science*, 4(10):3779–3804, 2011. 17

[79] Joel Henzie, Jeunghoon Lee, Min Hyung Lee, Warefta Hasan, and Teri W Odom. Nanofabrication of plasmonic structures. *Annual review of physical chemistry*, 60, 2009. 17

[80] John D. Joannopoulos, Steven G. Johnson, Joshua N. Winn, and Robert D. Meade. *Photonic Crystals: Molding the Flow of Light (Second Edition)*. Princeton University Press, 2 edition, 2008. ISBN 0691124566. 17

[81] Victor Veselago, Leonid Braginsky, Valery Shklover, and Christian Hafner. Negative refractive index materials. *Journal of Computational and Theoretical Nanoscience*, 3(2):189–218, 2006. 17

[82] Elliot W Hawkes, Eric V Eason, David L Christensen, and Mark R Cutkosky. Human climbing with efficiently scaled gecko-inspired dry adhesives. *Journal of The Royal Society Interface*, 12(102): 20140675, 2015. 17

[83] Alejandro Rodriguez, Alexander McCauley, David Woolf, Federico Capasso, John D. Joannopoulos, and Steven G Johnson. Nontouching nanoparticle diclusters bound by repulsive and attractive casimir forces. *Physical review letters*, 104:160402, 04 2010. 18

[84] Maofeng Dou, Fei Lou, Mathias Boström, Iver Brevik, and Clas Persson. Casimir quantum levitation tuned by means of material properties and geometries. *Physical Review B*, 89(20):201407, 2014. 18

[85] Norio Inui. Quantum levitation of a thin magnetodielectric plate on a metallic plate using the repulsive casimir force. *Journal of Applied Physics*, 111(7):074304, 2012. 18

[86] R Zhao, J Zhou, Th Koschny, EN Economou, and CM Soukoulis. Repulsive casimir force in chiral metamaterials. *Physical review letters*, 103(10):103602, 2009. 18

[87] Qing-Dong Jiang and Frank Wilczek. Chiral casimir forces: Repulsive, enhanced, tunable. *Physical Review B*, 99(12):125403, 2019. 18

[88] Johan S Høye and Iver Brevik. Casimir force between ideal metal plates in a chiral vacuum. *The European Physical Journal Plus*, 135(2):1–5, 2020. 18

[89] Ulf Leonhardt and Thomas G Philbin. Quantum levitation by left-handed metamaterials. *New Journal of Physics*, 9(8):254, 2007. 18

[90] Norio Inui. Temperature dependence of the casimir force between a superconductor and a magnetodielectric. *Physical Review A*, 86 (2):022520, 2012. 18

[91] Norio Inui and Kouji Miura. Quantum levitation of graphene sheet by repulsive casimir forces. *e-Journal of Surface Science and Nanotechnology*, 8:57–61, 2010. 18

[92] Francesco Intravaia, Stephan Koev, Il Woong Jung, A Talin, Paul Davids, Ricardo Decca, Vladimir Aksyuk, Diego A R Dalvit, and Daniel Lopez. Strong casimir force reduction through metallic surface nanostructuring. *Nature Communications*, 4:2515, 09 2013. 18

[93] Gauthier Torricelli, Peter J Van Zwol, Olex Shpak, George Palasantzas, Vitaly B Svetovoy, Chris Binns, Bart J Kooi, Peter Jost, and Matthias Wuttig. Casimir force contrast between amorphous and crystalline phases of aist. *Advanced functional materials*, 22(17): 3729–3736, 2012. 18

[94] F Chen, GL Klimchitskaya, VM Mostepanenko, and U Mohideen. Demonstration of optically modulated dispersion forces. *Optics Express*, 15(8):4823–4829, 2007. 18

[95] F Chen, GL Klimchitskaya, VM Mostepanenko, and U Mohideen. Control of the casimir force by the modification of dielectric properties with light. *Physical review B*, 76(3):035338, 2007. 18

[96] Jing Wang, Xiangdong Zhang, Shou-Yong Pei, and Da-He Liu. Tunable casimir forces by means of the external magnetic field. *Physical Review A*, 73(4):042103, 2006. 18

[97] F Pinto. Computational considerations in the calculation of the casimir force between multilayered systems. *International Journal of Modern Physics A*, 19(24):4069–4084, 2004. 24

[98] Marin-Slobodan Tomas. Green function for multilayers: Light scattering in planar cavities. *Phys. Rev. A*, 51, 03 1995. 28

[99] Christian Raabe, Ludwig Knöll, and Dirk-Gunnar Welsch. Three-dimensional casimir force between absorbing multilayer dielectrics. *Physical Review A*, 68, 12 2002. 28

[100] B. E. Sernelius. Electromagnetic normal modes and casimir effects in layered structures. *Physical Review B*, 90:155457, 2014. 28

[101] VB Svetovoy, PJ Van Zwol, G Palasantzas, and J Th M De Hosson. Optical properties of gold films and the casimir force. *Physical Review B*, 77(3):035439, 2008. 31, 36

[102] Kevin M McPeak, Sriharsha V Jayanti, Stephan JP Kress, Stefan Meyer, Stelio Iotti, Aurelio Rossinelli, and David J Norris. Plasmonic films can easily be better: rules and recipes. *ACS photonics*, 2(3):326–333, 2015. 31

[103] David B Hough and Lee R White. The calculation of hamaker constants from liftshitz theory with applications to wetting phenomena. *Advances in Colloid and Interface Science*, 14(1):3–41, 1980. 31

[104] V Adrian Parsegian. *Van der Waals forces: a handbook for biologists, chemists, engineers, and physicists*. Cambridge University Press, 2005. 31

[105] P. J. van Zwol and G. Palasantzas. Repulsive casimir forces between solid materials with high-refractive-index intervening liquids. *Phys. Rev. A*, 81:062502, Jun 2010. 31, 32

[106] U Strom, J.R. Hendrickson, R.J. Wagner, and P.C. Taylor. Disorder-induced far infrared absorption in amorphous materials. *Solid State Communications*, 15:1871–1875, 12 1974. 32

[107] Rei Kitamura, Laurent Pilon, and Miroslaw Jonasz. Optical constants of silica glass from extreme ultraviolet to far infrared at near room temperature. *Applied Optics*, 46:8118–33, 11 2007. 32

[108] T Inagaki, E T. Arakawa, R N. Hamm, and M W. Williams. Optical properties of polystyrene from the near infrared to the x-ray region and convergence of optical sum rules. *Phys. Rev. B*, 15, 03 1977. 32

[109] William R. Folks, Sidhartha K. Pandey, Greg Pribil, W Dennis Slafer, Monis Manning, and Glenn Boreman. Reflective infrared

ellipsometry of plastic films. *International Journal of Infrared and Millimeter Waves*, 27:1553–1571, 11 2006. 32

[110] Michael Elbaum and M Schick. Application of the theory of dispersion forces to the surface melting of ice. *Physical review letters*, 66(13):1713, 1991. 33, 34, 35

[111] RS Decca, D López, E Fischbach, GL Klimchitskaya, DE Krause, and VM Mostepanenko. Precise comparison of theory and new experiment for the casimir force leads to stronger constraints on thermal quantum effects and long-range interactions. *Annals of Physics*, 318(1):37–80, 2005. 36, 38

[112] Brunero Cappella and Giovanni Dietler. Force-distance curves by atomic force microscopy. *Surface science reports*, 34(1-3):1–104, 1999. 37

[113] V Adrian Parsegian and David Gingell. On the electrostatic interaction across a salt solution between two bodies bearing unequal charges. *Biophysical journal*, 12(9):1192–1204, 1972. 37

[114] Cyriaque Genet, Astrid Lambrecht, P Maia Neto, and Serge Reynaud. The casimir force between rough metallic plates. *EPL (Europhysics Letters)*, 62(4):484, 2003. 38

[115] Paulo A Maia Neto, Astrid Lambrecht, and Serge Reynaud. Casimir effect with rough metallic mirrors. *Physical Review A*, 72(1):012115, 2005. 38

[116] PA Maia Neto, Astrid Lambrecht, and Serge Reynaud. Roughness correction to the casimir force: Beyond the proximity force approximation. *EPL (Europhysics Letters)*, 69(6):924, 2005. 38

[117] Georgios Palasantzas and J Th M De Hosson. Pull-in characteristics of electromechanical switches in the presence of casimir forces: Influence of self-affine surface roughness. *Physical Review B*, 72(11):115426, 2005. 38

[118] PJ Van Zwol, G Palasantzas, and J Th M De Hosson. Roughness corrections to the casimir force: The importance of local surface slope. *Applied Physics Letters*, 91(14):144108, 2007. 38

[119] PJ Van Zwol, G Palasantzas, and J Th M De Hosson. Influence of random roughness on the casimir force at small separations. *Physical Review B*, 77(7):075412, 2008. 38

[120] Wijnand Broer, George Palasantzas, Jasper Knoester, and Vitaly B Svetovoy. Roughness correction to the casimir force at short separations: Contact distance and extreme value statistics. *Physical Review B*, 85(15):155410, 2012. 38

[121] CC Speake and C Trenkel. Forces between conducting surfaces due to spatial variations of surface potential. *Physical review letters*, 90 (16):160403, 2003. 39

[122] RO Behunin, F Intravaia, DAR Dalvit, PA Maia Neto, and S Reynaud. Modeling electrostatic patch effects in casimir force measurements. *Physical Review A*, 85(1):012504, 2012. 39

[123] Joseph L Garrett, David Somers, and Jeremy N Munday. The effect of patch potentials in casimir force measurements determined by heterodyne kelvin probe force microscopy. *Journal of Physics: Condensed Matter*, 27(21):214012, 2015. 39

[124] RO Behunin, DAR Dalvit, RS Decca, C Genet, IW Jung, A Lambrecht, A Liscio, D López, S Reynaud, G Schnoering, et al. Kelvin probe force microscopy of metallic surfaces used in casimir force measurements. *Physical Review A*, 90(6):062115, 2014. 39

[125] Pochi Yeh et al. *Optical waves in layered media*, volume 95. Wiley New York, 1988. 39

Instituto de Ciencia de Materiales de Sevilla, 2021

CSIC
CONSEJO SUPERIOR DE INVESTIGACIONES CIENTÍFICAS

MOM
mom.icmse.csic.es
Multifunctional
Optical
Materials
Group

UNIVERSIDAD DE SEVILLA

"la Caixa" Foundation